An Interacting Quantum Fragments-rooted Preorganized-interacting Fragments Attributed Relative Molecular Stability of the Be^{II} Complexes of Nitrilotriacetic Acid and Nitrilotri-3-propionic Acid

Ignacy Cukrowski and Paidamwoyo Mangondo*

Department of Chemistry, Faculty of Natural and Agricultural Sciences, University of Pretoria, Lynnwood Road, Hatfield, Pretoria 0002, South Africa

*Corresponding author:

E-mail: ignacy.cukrowski@up.ac.za

Landline: +27 12 420 3988

Fax: +27 12 420 4687

Abstract

A method designed to investigate, on a fundamental level, the origin of relative stability of molecules (or molecular systems in general) using Be^{II} complexes with nitrilotriacetic acid (NTA) and nitrilotri-3-propionic acid (NTPA) as a case study (this is the only known example where a metal ion forms stronger complex with NTPA) is described. It makes use of the primary (self-atomic and diatomic interaction) and molecular fragment energy terms as defined in the IQA/F (Interacting Quantum Atoms/Fragments) framework. An extensive classical-type investigation, focused on single descriptors (bond length, density at critical point, the size of metal ion or coordination ring, interaction energy between Be^{II} and a donor atom, etc.) showed that it is not possible to explain the experimental trend. The proposed methodology is fundamentally different in that it accounts for the total energy contributions coming from all atoms of selected molecular fragments, and monitors changes in defined energy terms (*e.g.*, fragment deformation, inter- and intra-fragment interaction) on complex formation. By decomposing combined energy terms we identified the origin of relative stability of Be^{II}(NTA) and Be^{II}(NTPA) complexes. We found that the sum of coordination bonds' strength, as measured by interaction energies between Be^{II} ion and donor atoms, favours BeNTA but the binding energy of Be^{II} ion to the entire ligand correlates well with experimental trend. Surprisingly, the origin of Be^{II}(NTPA) being more stable is due to less severe repulsive interactions with the backbone of NTPA (C and H-atoms). This general purpose protocol can be employed not only to investigate the origin of relative stability of any molecular system (*e.g.*, metal complexes) but, in principle, can be used as a predictive tool for, *e.g.*, explaining reaction mechanism (transitional states).

1. Introduction

Metal ions in solution have an almost inexhaustible list of applications which vary from catalysis, to medicine, to biological use, to extraction metallurgy. At the core of understanding the behaviour of metal ions in solution is the use and determination of formation constants.[1] Formation constants can reveal factors and trends influencing ligand design and metal ion selectivity, which are both appealing to chemists. Extensive experimental investigations have been dedicated to the determination of protonation and formation constants resulting in detailed databases recording this data.[2] However, the experimental data do not provide sufficient insight into the nature of interactions, describe chelating effect or provide any additional insight into the factors controlling the affinity between metal ions and donor ligands.[3,4] In order to gain additional insight, the thermodynamic constants have been the subject of theoretical investigation. Attempts have been made to predict the dissociation constants of ligands[5–20] theoretically, linear free-energy relationships (LFER) have been used to predict the formation constants of metal complexes,[21,22] and the formation constants for Ni^{II} complexes of NTA and NTPA have been successfully predicted using competition reactions.[3]

While this information is insightful as it identifies (in many cases) trends in the stability of metal complexes, it still fails to provide a fundamental understanding of the relative stability of metal complexes. This is evident in the failure to explain the change in the stability of complexes when small changes are made to the ligand structure. A classic example is the preferential complex formation of metal ions to form five-member chelate rings (5m-CR) when compared to six-membered chelate rings (6m-CR) except when binding to small metal cations.[1,23] The complexes of nitrilotri-3-propionic acid (NTPA, it forms 6m-CR) and nitrilotriacetic acid (NTA, it forms 5m-CR) are characteristic examples of this phenomenon. NTA, which forms strong complexes with most metal ions, is known as an alternative detergent builder[24] and is used in Ni-NTA-gold clusters to target tagged proteins.[25] On the other hand NTPA, has very few uses because it forms weak complexes. Be^{II}, a small metal ion with ionic radius 0.27 Å,[26] is the only known example of preferential complex formation with NTPA with three 6m-CRs ($\log K_1$ = 9.23 at 25 °C, μ = 0.5 M $NaNO_3$)[2] when compared to NTA which forms three 5m-CRs ($\log K_1$ = 6.84 at 25 °C, μ = 0.5 M $NaNO_3$),[2] resulting in $\Delta\log K_1 \approx 2.4$ in favour of Be^{II}(NTPA). The opposite is true for numerous larger metal ions, including Zn^{II} which has an ionic radius of 0.74 Å.[26] Zn^{II} will preferentially complex to NTA ($\log K_1$ = 10.45 at 25 °C, μ = 0.1 M KCl) [2] rather than NTPA ($\log K_1$ = 5.3 at 25 °C, μ = 0.1 M KNO_3)[2], with $\Delta\log K_1 \approx 5.1$.

Classically, complex stability is said to be governed by repulsion between lone-pair donors (such as oxygen and nitrogen), steric repulsion between crowded atoms, the size of the metal cation, coordination bond strength as measured by its length and to a lesser extent, inductive effects.[1,23] Furthermore, the differences in the formation constants of many complexes have been attributed to repulsive H-clashes due to the presence of the CH--HC close contacts.[1,27–31] Although this is not the main focus of this work, these CH--HC close contacts are also observed in systems investigated here. This notion was challenged by Bader using the Quantum Theory of Atoms in Molecules (QTAIM).[32] QTAIM uses electron density to analyse different types of interactions, where the presence of a ridge of maximum electron density linking two atoms is defined as an atomic interaction line (AIL), which Bader interpreted as a bonding interaction, hence a bond path (BP).[33] While QTAIM has been able to recover BPs where a classical chemical bond is expected, it has also shown the presence of AILs where steric hindrance is classically expected,[34–42] thus a debate has ensued discussing the meanings and interpretations of chemical bonds, steric repulsions and the concept of bonding.[31,33,43–57] Despite this controversy, QTAIM has been widely used for the visualization and analysis of all kinds of chemical bonds in a variety of compounds, among them coordination bonds and intramolecular interactions in various metal complexes.[3,4,57–61] For the complexes of Ni^{II} and Zn^{II} with NTA and NTPA,[3,4] the following was determined: (i) BPs where found for the weak CH•••HC and CH•••O intramolecular interactions in the complexes of NTPA, (ii) the density at the ring critical point (RCP) of a chelating ring appeared to correlate with the differences in the formation constants between 5m-CR and 6m-CR complexes, and (iii) the differences in formation constants were attributed to the greater strain incurred during the preorganization of NTPA with the ratio of the strain energy of NTPA:NTA being comparable to the ratio of the formation constants.

This work presents a comprehensive study of the factors controlling the stability of metal complexes, using Be^{II}(NTA) and Be^{II}(NTPA) complexes (for brevity they have been represented as BeNTA and BeNTPA respectively) as a case study because, to our knowledge, (i) they have not been extensively investigated computationally and (ii) this is the only case when log K_1 is larger for the BeNTPA complex. A competition reaction is used here to select an appropriate level of theory for solvent optimized complexes based on the quality of the prediction of experimental formation constants as well as the computed trend in molecular energies. We then examine a full battery of local, real space indices and techniques that include: (i) geometrical analysis to evaluate coordination bond strength and steric strain, (ii) topological properties, using QTAIM,[32] in both complexes, which characterize and measure the strength of the BP-linked intramolecular interactions with the hope that it would explain the experimental trend in complex stability, (iii) NCI (Non-Covalent Interactions)[62–65] isosurfaces which visualize all intramolecular interactions with our focus on those interactions which are not recovered by QTAIM, and (iv) strength as well as physical nature and quantified (de)stabilizing energy contribution of selected interactions using the Interacting Quantum Atoms (IQA)[66–68] energy decomposition scheme. We then use an intuitive, general-purpose approach to investigate complex (or more generally molecular system) stability, where we recognize that complex formation is a process and we apply a simplified two stage model (ligand preorganization and the binding between the pre-organized ligand and metal ion) to simulate the process of complex formation. We then investigate the fundamental properties and factors controlling the two stages by using the QTAIM, NCI and IQA techniques. In the final section we will present a method, that is deeply rooted in IQA and the Interacting Quantum Fragments (IQF),[68] which gives one the ability to explore and identify the factors affecting stability of a molecular system by dividing a molecule into chemically meaningful fragments and analysing the interaction energy between them; all implemented without artificially dissecting the molecules investigated here. To our knowledge, this is the first attempt of this kind in explaining the processes of preorganization, binding and relative stability of molecular systems. In addition, we have also investigated the suitability of selected DFT techniques for the purpose of such studies using MP2 as a reference.

2. Computational Details

The free ligands of NTA and NTPA, as well as the Be^{II} complexes were submitted for a full conformational search in Spartan 10.[69] Geometry optimizations of the SPARTAN generated conformers (ligands and complexes) as well as of the free beryllium cation were performed in Gaussian 09 revision D,[70] at the MP2(FC) levels of theory; Cartesian coordinates for all structures obtained at indicated levels of theory are presented in Tables S10-S13 in the Supplementary Information. In order to have the structural benefit of the MP2-optimized structures, as well as Gibbs free energies needed to predict formation constants, but to minimize the computational expense, single point frequency calculations (SPFC) were carried out on the MP2 optimized structures at PBE1PBE, B3LYP and X3LYP. To evaluate the processes involved in complex formation, single point energy calculations were performed at all levels of theory on the pre-organized ligand, $\mathcal{L}_{\text{p-org}}$ (ligand with the structure observed in the complexes of beryllium). All optimizations and single point calculations were performed with the 6-311++G(d,p) basis set in the PCM/UFF solvation model with water as the solvent. Selected wavefunctions were submitted for topological analysis and for the determination of IQA defined properties using the AIMAll package.[71] We must stress here that regardless of the level of theory, the change in the energy of a molecule recovered from the IQA additive atomic energies, *e.g.*, when a ligand changed from its free to pre-organized form, always followed the trend but differ somewhat in value. This is fully understandable because (i) an accurate implementation of IQA requires well-defined second order density matrix but, unfortunately, it is not implemented in AIMAll software for post HF levels of theory (including MP2) yet – instead, the Müller approximation of the two-electron density matrix in terms of natural orbitals of the one-electron density matrix is used; (ii) numerous energy components contribute to the IQA-defined molecular energy, E, and small numerical integration errors (a numerical 'noise') are unavoidable regardless. As such, even the IQA data at the MP2 level of theory, presented in this work is also an approximation in the AIMAll software. Furthermore, because our focus is on relative trends rather than predicting energy terms on an absolute scale, we are convinced that the qualitative results and the conclusions arrived at from this work should be considered as valid. For our purposes we often made use of the X3LYP wavefunction computed on the MP2-optimized structure because (i) all DFT calculations gave good approximations of the electronic energy obtained for the competition reaction, (ii) it has been shown recently that IQA calculations on a DFT wavefunction give reasonable approximations of computationally expensive MP2 data,[72] and (iii) X3LYP is known to describe weak inter- and intra-molecular interactions[73–76] and the structure and electronic properties of molecular systems[73,76–78] in a well-defined manner. In some instances we performed MP2 computations needed to directly verify DFT results. Either NCIPlot 2.0[63] was used for the determination of isosurfaces in combination with VMD 1.9.1[79] used for their visualization, or AIMAll was employed for that purpose. One dimensional cross-sections of the electron density along the λ_2 eigenvector of the Hessian matrix were performed using in-house software according the procedure detailed previously.[80]

3. Results and Discussion

3.1. Preliminary Investigations

Before imbarking on any detailed investigations it was necessary to validate the structures generated for analysis. To this effect, a competition reaction, CRn = BeNTA + NTPA ↔ BeNTPA + NTA, and a corresponding equilibrium constant, K_1^{CRn}, were used. For convenience, major steps of the CRn-based protocol (it was reported and examined in details previously[3]) as well as results relevant to this work obtained at different levels of theory are included in PART 1 of the Supplementary Information. The preferential formation of BeNTPA, with $\log K_1^{\mathrm{CRn}}$ = 4.7, has been fully recovered at the MP2 level of theory when the Gibbs free energies of the lowest energy conformers, LECs, of NTA and NTPA (Figure S1 in the SI) and LECs of BeNTA/BeNTPA complexes (their ball-and-stick representation, together with the implemented notation and numbering of atoms, is shown in Figure 1) were used. The experimental trend in relative stability of BeNTA and BeNTPA complexes was also recovered at all DFT-levels of theory tested here (for details see PART 1 in the SI) and for the QTAIM, NCI and IQA analyses the X3LYP wavefunctions (obtained from the single point calculations on the MP2-optimized structures) were selected.

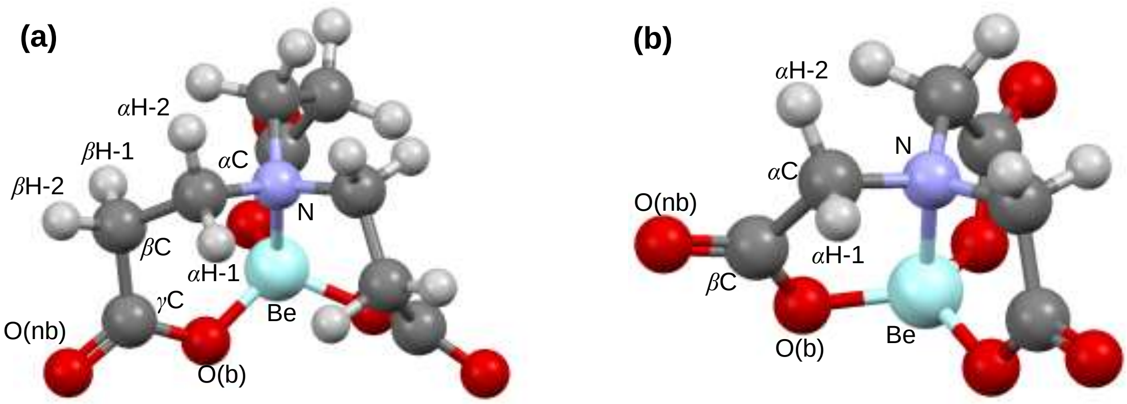

Figure 1. Ball-and-stick representation of the LECs of (a) BeNTPA, and (b) BeNTA, also showing notation used and numbering of atoms.

The good approximation of the $\log K_1^{\mathrm{CRn}}$ and ΔE_{CRn} gave us the confidence to use the MP2 optimized structures and X3LYP-generated wavefunctions in the analysis of numerous individual descriptors commonly employed to explain the relative stability of complexes, or molecular systems in general. These were: (i) geometric properties, such as interatomic distances, bite angles, etc. (ii) numerous topological properites at the selected critical points as determined from QTAIM – molecular graphs of Be^{II} complexes are shown in Figure 2, (iii) the NCI-isosurfaces used to aid interpretation of intramolecular interactions, intramolecular strain and to identify additional and QTAIM-missed intramolecular non-covalent interactions – see Figure 3, and (iv) the IQA-defined diatomic interaction energies needed to quantify strengths of interactions of interest (the full set of computed data and the detailed interpretation is included in PART 2 of the SI). A great deal of physical insight can be obtained from this information however, to remain within limits of the paper this material has been transferred to the SI.

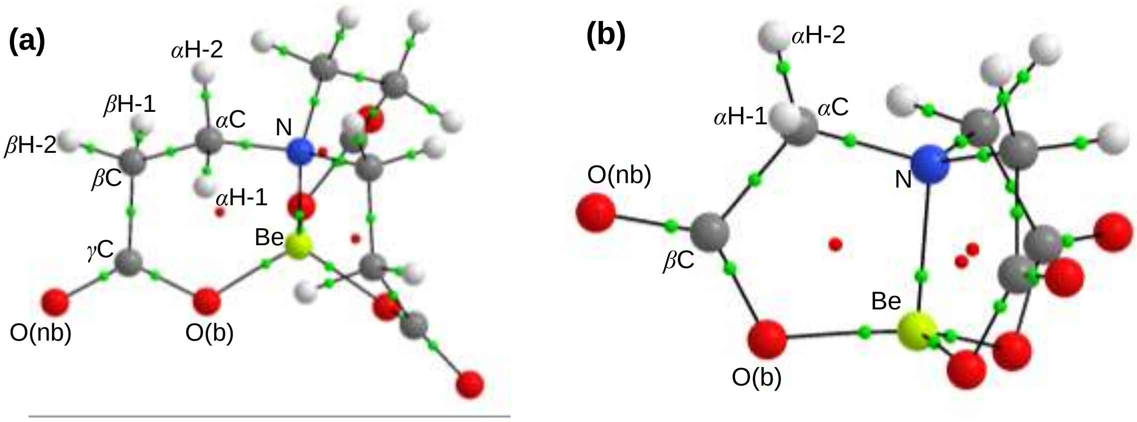

Figure 2. The QTAIM molecular graphs of the lowest energy conformers of (a) BeNTPA, and (b) BeNTA.

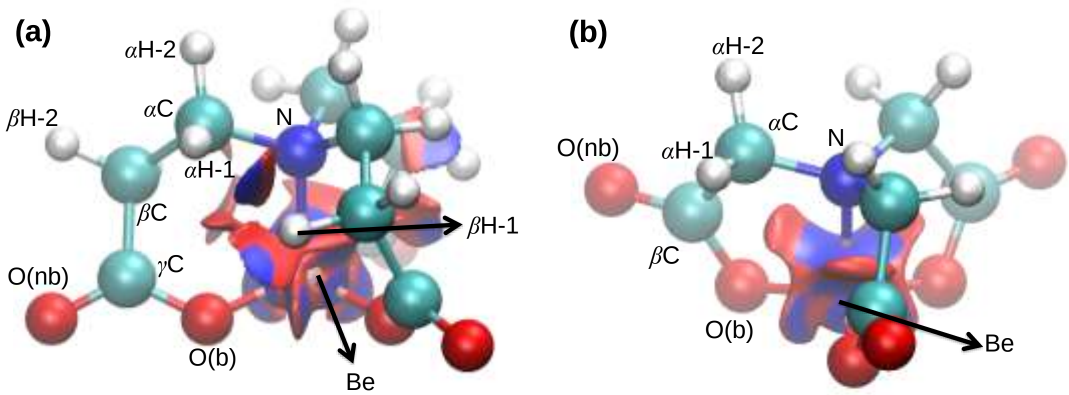

Figure 3. The NCI isosurfaces of the LECs of (a) BeNTPA, and (b) BeNTA complexes with a RDG isovalue of 0.5 au and isosurfaces coloured from blue to red using -0.07 au $\leq \mathrm{sign}(\lambda_2)\times\rho(r) \leq +0.03$ au.

Table 1 provides a comprehensive summary of numerous analyses performed from which, following classical interpretations, an orthodox chemist would hope to find factors controlling stability of these two molecular systems. In addition, we have included in Table 1 the most likely prediction made, based on common interpretations of individual properties, indicating that either BeNTA or BeNTPA are preferentially formed. Unfortunately, data shown in Table 1 clearly reveals that one is unable to provide a conclusive answer as seven out of eleven properties point at BeNTA as being more stable, contradicting experimentally established trend. Thus we came to the conclusion that further analyses of local indices most likely will be as fruitless and we decided to develop a protocol which should account for the combined effect of many components and this is the subject of sections that follow.

Table 1. Comprehensive overview of the properties investigated and, based on classical interpretation, prediction of more stable complex from the analysis of a single property.[a]

Complex	d(Be,N)	d(Be,O)	d(H,H)	$\rho_{\mathrm{BCP}}^{\mathrm{Be\text{-}N(O)}}$	ρ_{RCP}	$E_{\mathrm{int}}^{\mathrm{Be,N}}$	$E_{\mathrm{int}}^{\mathrm{Be,O}}$	Sum-1	$E_{\mathrm{int}}^{\mathrm{N,O}}$	$E_{\mathrm{int}}^{\mathrm{O,O}}$	Sum-2
	Å			au		kcal/mol					
BeNTPA	1.791	1.610	2.159	0.060 (0.075)	0.018	–424.3	–484.9	–1781	183.2	204.3	1229
BeNTA	1.772	1.612	2.331	0.064 (0.077)	0.034	–437.2	–484.3	–1791	196.9	197.3	1252
More stable:	NTA	NTPA	NTA	NTA	NTA	NTA	NTPA	NTA	NTPA	NTA	NTPA

[a] Sum-1 stands for summed interaction energies of all coordination bonds, Sum-2 stands for summed interaction energies between O and N atoms of the coordination spheres.

3.2. Preorganized-interacting Fragments Attributed Relative Molecular Stability: a π-FARMS Method.

One can discover the more stable conformer of a compound, or the most likely product of a chemical reaction (or more stable metal complex) by simply computing the energy of this compound formation, either ΔG or ΔE for the reaction of interest. However, this provides no insight whatsoever on why it is preferentially formed. Hence, our main aim is to develop, within an IQF-framework, a general purpose protocol which could be suitable to explain relative stability of molecular systems on a fundamental level providing an insight on the origin of the observed, either experimentally or theoretically predicted, trend. To this effect, and focussing on relative stability of metal complexes, we will consider the formation of a complex in aqueous environment as a result of two simplified (or imaginary) separate processes, (i) preorganization of molecular fragments and (ii) interaction between them, as depicted in Scheme 1.[81] Our approach involves the comparative study, hence we assumed that the large hydration spheres of all components involved (a real aqueous environment with many water molecules) can be neglected. One should also note that dissociation of $Be(H_2O)_n$ is the same process for both complexes, thus dissociation energy E_{diss} cancels off.

Scheme 1. A simplified decomposition of the complex formation process.

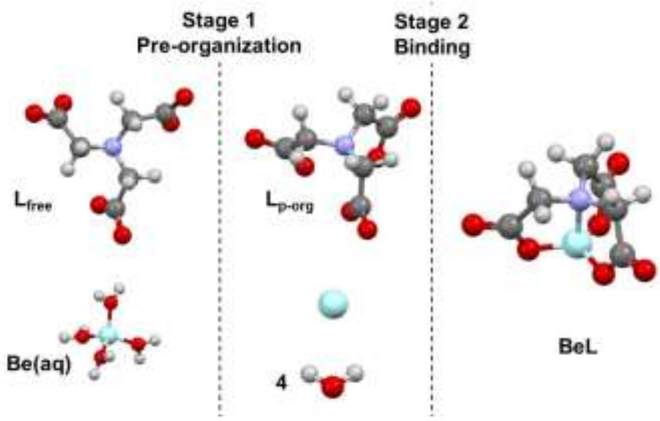

Let us focus now on two processes considered:

a) Stage 1 in Scheme 1 represents preorganization of a ligand, a necessary structural change leading from a free ligand structure $\mathcal{L}_f$ to that observed in a complex. This process requires an additional 'penalty' energy, called here a preorganization energy, $E^{\mathcal{L}}_{\text{p-org}}$, which must be different for both ligands, $E^{\text{NTA}}_{\text{p-org}} \neq E^{\text{NTPA}}_{\text{p-org}}$. By investigating this process one should gain an understanding of and an insight on the origin of strain in structures of pre-organized ligands, $\mathcal{L}_p$.

b) Stage 2 in Scheme 1 represents binding between $\mathcal{L}_p$ and Be, which leads to complex formation and associated E_{bind}, this can also be seen as a measure of affinity between a bare metal ion and $\mathcal{L}_p$. This process will be explored to uncover most significant energy components related to the origin of binding energy.

There is an additional advantage of this protocol, namely one can also compare variations occurring when $\mathcal{L}_p$ changes its fundamental physical properties to those when in a complex, $\mathcal{L}_c$. From this one should be able to gain an insight on how much and where a ligand is gaining/losing energy when coordination bonds are formed. Note that even though structurally $\mathcal{L}_p$ and $\mathcal{L}_c$ are identical, the atomic energies as well as intra-ligand and intra-complex interactions must be totally different. This is because only interactions within the ligand framework are taking place in $\mathcal{L}_p$ whereas the presence of Be will add many interactions as well as modify those within the framework of $\mathcal{L}_c$ relative to $\mathcal{L}_p$. Importantly, because the IQA-defined one- and two-body components will be accounted for, this should provide us with a total description of energy changes taking place. Furthermore, the geometry of atoms not involved in the coordination bond formation might also vary when a ligand changes from the $\mathcal{L}_f$ to $\mathcal{L}_p$ states and this can result in somewhat different (i) density distribution within atomic basins as well as (ii) net charge of these atoms. These two changes in the atoms' physical properties, in addition to their different 3D placement in the $\mathcal{L}_f$ to $\mathcal{L}_p$ states, will also contribute to the computed change in the interaction energy terms; hence, the geometric deformation energy of atoms not involved in the intramolecular interaction should be, although indirectly, accounted for to some extent.

Let us start our analysis from defining the preorganization energy, $E_{\text{p-org}}$, related to the first stage in Scheme 1

$$E_{\text{p-org}} = E(\mathcal{L}_p) - E(\mathcal{L}_f) \qquad (1)$$

and binding energy, E_{bind}, related to the second stage of the complex formation, which can be expressed as

$$E_{\text{bind}} = E(\text{BeL}) - E(\mathcal{L}_p) - E(\mathcal{M}_f) \qquad (2)$$

It is important to note that the sum of the two processes, in terms of the related energy contributions, $E_{\text{p-org}} + E_{\text{bind}}$, must amount to the resultant complex formation energy, $E_{\text{BeL}} = E(\text{BeL}) - E(\mathcal{L}_f) - E(\mathcal{M}_f)$, related to the reaction of the metal ion with the free ligand, $\mathcal{M}_f + \mathcal{L}_f = \text{BeL}$. The nuance in this approach is that rather than defining relative complex stability based on selected individual properties (indicated in Table 1) of the final product (the BeL structure), we recognize complex formation as a process. This can be seen as a paradigm shift in the field of studying metal complexes as the combined changes in physical and energetic properties throughout the complex formation processes will be under scrutiny as this should bear more weight and information on the relative stability of a molecular systems formed. This, IQF-based, approach is also different to the ETS-NOCV method[82-84] which was utilized previously[4] in the study of Zn complexes with NTA and NTPA ligands. While ETS-NOCV has been useful in understanding overall changes in the molecular system, it could not provide an insight on the origin of computed energy terms at the atomic, molecular fragment, interatomic and interfragment levels. Furthermore, in our approach, real molecular fragments are used rather than radicals obtained from dissections of a ligand into unphysical, hence non-existing, components.

Table 2. Computed preorganization energies and binding energies (all in kcal/mol) using relevant energy terms obtained for $\mathcal{L}_f$ and $\mathcal{L}_p$ of NTA/NTPA, and the BeNTA/ BeNTPA complexes.

Level of Theory	$E_{p\text{-}org}$				E_{bind}				ΔE_{ML} [a]
	NTA	NTPA	$\Delta E_{p\text{-}org}$[b]	Ratio[c]	BeNTA	BeNTPA	ΔE_{bind}[d]	Ratio[c]	
MP2[e]	52.0	61.2	9.2	1.2	–266.5	–284.5	–18.0	1.1	–8.8
PBE1PBE[f]	53.7	67.7	14.0	1.3	–264.4	–283.0	–18.6	1.1	–4.7
B3LYP[f]	53.5	69.5	16.0	1.3	–268.8	–287.4	–18.6	1.1	–2.7
X3LYP[f]	53.2	68.6	15.4	1.3	–270.5	–289.2	–18.7	1.1	–3.4

[a] $\Delta E_{ML} = E_{BeNTPA} - E_{BeNTA}$; [b] $\Delta E_{p\text{-}org} = E_{p\text{-}org}(\text{NTPA}) - E_{p\text{-}org}(\text{NTA})$; [c] Ratio = (NTPA/NTA) value; [d] $\Delta E_{bind} = E_{bind}(\text{BeNTPA}) - E_{bind}(\text{BeNTA})$; [e] energies were obtained by optimizing the lowest energy conformer of each molecule; [f] electronic energy obtained by performing a single point calculation on the MP2 structure at the indicated level of theory.

The results in Table 2 show that both ligands needed additional and significant energy (*e.g.*, 52 kcal/mol in case of NTA at MP2) to attain the geometry observed in complexes. We found that energy required to preorganize a ligand, $\Delta E_{p\text{-}org}$, is ~9 kcal/mol smaller for NTA (at MP2), probably because of smaller number of atoms involved. Importantly, this trend is consistent with the strain energies found for the same ligands forming zinc and nickel complexes.[3,4] As one would expect, the affinity of the metal ion to the pre-organized ligand (either NTA or NTPA) is such that the energy released on the complex formation (either BeNTA or BeNTPA) overrides the energy penalty incurred to pre-organize the ligand, with $\Delta E_{bind} = E_{bind}(\text{BeNTPA}) - E_{bind}(\text{BeNTA})$ of about –18 kcal/mol. This is important finding as it clearly demonstrates higher affinity of Be^{II} to NTPA. Furthermore, considering the the overall energy change, ΔE_{BeL}, which is related to the CRn involved (BeNTA + NTPA ↔ BeNTPA + NTA) we recovered the experimental trend at all levels of theory, *e.g.*, at the X3LYP level, $\Delta E_{BeL} = \{E_{p\text{-}org}(\text{NTPA}) + E_{bind}(\text{BeNTPA})\} - \{E_{p\text{-}org}(\text{NTA}) + E_{bind}(\text{BeNTA})\} =$ –3.4 kcal/mol. As a matter of fact, the relative complex formation energy, ΔE_{BeL}, which was obtained from Scheme 1 by partitioning the complex formation reaction into two processes, is equal to the ΔE_{CRn} value, *i.e.*, $\Delta E_{p\text{-}org} + \Delta E_{bind} = \Delta E_{BeL} = \Delta E_{CRn}$, obtained at each level of theory, thus reinforcing the employed protocol. Because of that and the fact that the DFT data qualitatively agreed with the MP2 ones we were able to explore the origins of energy changes related to each separate stage in Scheme 1 using electronic energy partitioning schemes, such as QTAIM/IQA.

3.2.1. Exploring the pre-organization (strain) energy of the ligands

In the previous section, we decomposed the process of complex formation into the preorganization (strain) energy and the binding energy between Be^{2+} and $\mathcal{L}_p$. We will first look at the changes which occurred in the ligand molecules on the preorganization step from the QTAIM perspectives - the molecular graphs of the $\mathcal{L}_{p\text{-org}}$ structures (NTPA and NTA) are shown in Figures 4(a,b).

Surprisingly, despite the presence of the highly repulsive environment (due to proximity of highly negatively charged O- and N-atoms within the coordination spheres) there are AILs present between donor atoms. We found ρ_{BCP}(O--O) of 0.0139 and 0.0153 au in NTA and NTPA, respectively, and these values are of the same order of magnitude as found for a classical intermolecular H-bond between two water molecules.[80] It is then rather difficult to interpret the observed AILs in terms of the classical meaning of QTAIM-defined bond paths. However, one might attempt to rationalize the appearance of these AILs as a way of decreasing repulsive forces between atoms involved by specific dissipation of electron density within the coordination sphere. This should and indeed results in (as shown in Table 3) the decrease in the electron population of atoms directly involved in steric clashes.

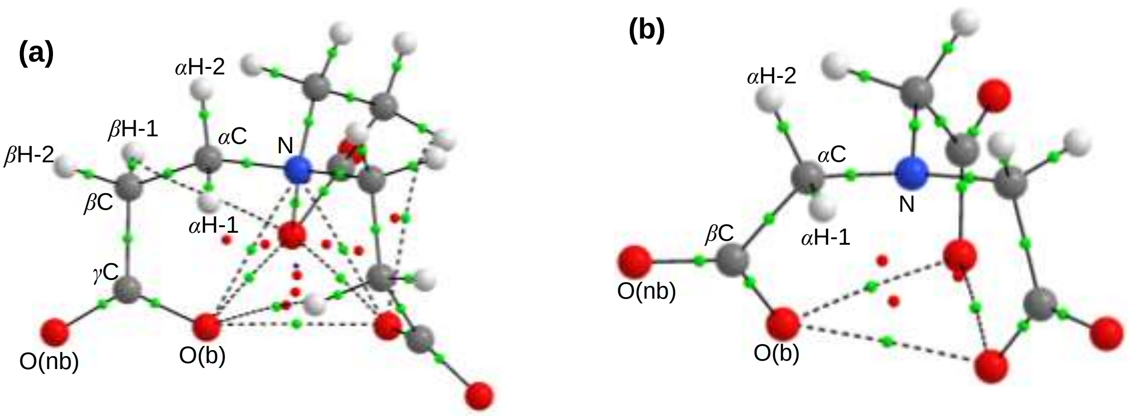

Figure 4. The QTAIM molecular graphs of pre-organized ligands as found in the (a) BeNTPA and (b) BeNTA complexes.

We also note that (i) there are no AILs present in the case of the N--O contacts in the pre-organized structure of NTA but there are three of them in NTPA with ρ_{BCP}(N--O) = 0.0163 au and (ii) there are additional AILs in the pre-organized form of NTPA which represent typical hydrogen bonds between O(b)-atoms and the βH atoms with ρ_{BCP}(O--H) = 0.0050 au; therefore, they might be seen as an orthodox bond paths (BPs). In general, molecular graphs in Figure 4 can be seen as a classical example showing how a molecular system responds to the structural change from fully relaxed (lowest energy state) to highly crowded 3-D atoms distribution. It appears that an AIL is formed not only when a classical chemical bond is formed (then, following a chemist's intuition it is appropriate to call such AIL a BP) but also might be formed to minimize an anavoidble energy penalty caused by highly crowded and repulsive coordination sphere, as observed in the studied complex. Regardless of the origin of the AIL appearance, in both cases the presence of AILs is minimizing the system's energy. This is accomplished by either (i) forming a chemical bond (which is always of stabilizing nature) or (ii) partly reducing molecule's instability due to the contribution made by the always negative XC-term (associated with an atomic interaction line) which, in turn, is minimizing positive energy attributed to intra-coordination sphere strain. This observation not only correlates well with Bader's view that "For a system in a stationary state, the wavefunction and the electron density it determines are such as to minimize the total energy."[85] but it also extends his interpretation to a transitional state.

As expected, the NCI isosurfaces shown in Figure 5 fully recover the QTAIM molecular graphs, indicating blue regions of electron density accumulation at BCPs where AILs were present and red cigar-shaped isosurfaces (elongated along directions of increasing density) with the thickest middle part coinciding with RCPs on molecular graphs. Very intriguing isosurfaces are observed between O-atoms involved in the steric clash in NTPA; blue-coloured discs are observed (without a trace of red surrounding area, which is synonymous with stabilizing interaction in classical NCI interpretations, *e.g.*, this is exactly the picture which one observes for classical intramolecular H-bond (see Figure S6 in Supplementary Information).

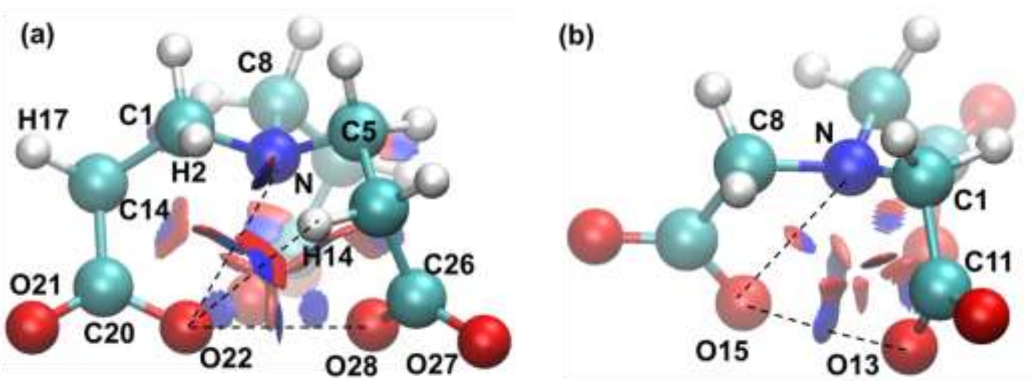

Figure 5. The NCI isosurfaces of (a) $\mathcal{L}_{\text{p-org}}$(NTPA), and (b) $\mathcal{L}_{\text{p-org}}$(NTA), with a RDG isovalue of 0.5 au and isosurfaces coloured from blue to red using -0.07 au $\leq \text{sign}(\lambda_2)\times\rho(r) \leq$ +0.03 au.

To rationalize this observation one might speculate that in this particular case it simply represents an overlap of orbitals with free pairs of electrons and this does not require a density re-arrangement which explains why we do not see red coloured isosurfaces. There are only three AILs in the pre-organized NTA but the NCI revealed the presence of additional bi-centric isosurfaces; a red area directly between N- and O(b)-atoms with an adjacent blue region placed outside the ring. Because density was removed from the interatomic region (thus NCI-interpreted repulsion), this might suggest that there was an 'excess' of density within the ring and, as a result, an adjacent blue region was formed which signifies the output of the redistributed excess electron density in the highly crowded environment. In general, all the isosurfaces shown in Figure 5 illustrate how density has been arranged in highly strained coordination sphere of the two ligands.

The origin of pre-organization energies. There are many, complex features observed in both, the NCI isosurfaces and molecular graphs, but their interpretation is far from trivial and intrinsically might be highly speculative. Because of that, we decided to trace the origin of preorganization energies from the IQA-perspectives using NCI isosurfaces as a useful guide. Furthermore, because the energy of a molecule is the sum of the additive energies of each atom, this allows identifying atoms that have made the greatest (de)stabilizing contribution to the change of the molecule's energy when $\mathcal{L}_{\mathrm{f}}$ changes to $\mathcal{L}_{\mathrm{p}}$, *e.g.*, atoms which are involved in highly repulsive environment (hence the classically interpreted steric strain) should experience a large increase in the additive atomic energy, $\Delta E_{\mathrm{add}}^{\mathrm{X}} > 0$, and become highly destabilized.

Data shown in Table 3 reveals that order(s) of magnitude larger changes in $\Delta E_{\mathrm{add}}^{\mathrm{X}}$ (they affect the $E_{\text{p-org}}$ value) occurred on the nitrogen atoms and all atoms of the carboxylate groups. Furthermore, the variation in the additive atomic energies, $\Delta E_{\mathrm{add}}^{\mathrm{X}}$ (when a ligand changed from the $\mathcal{L}_{\mathrm{f}}$ to $\mathcal{L}_{\mathrm{p}}$ state) shows that far more significant changes took place in NTPA. However, regardless of the magnitude of changes, there appears to be a consistent pattern in both ligands: the highly negatively charged atoms, N, O(b) and O(nb), experienced a large increase in atomic additive energies whereas the highly positively charged C-atoms of the carboxylate groups became stabilized the most.

Table 3. Relative to $\mathcal{L}_f$ structures, changes in the selected QTAIM (at the MP2 level of theory) and IQA (at the RX3LYP level of theory on the MP2 structure) energy terms (in kcal/mol) and additional properties of atoms in the pre-organized NTPA and NTA ligand.[a]

Atom X	$\Delta E_{\text{add}}^{\text{X}}$	$0.5\sum_{\text{Y}\neq\text{X}}\Delta E_{\text{int}}^{\text{X,Y}}$	$\Delta E_{\text{self}}^{\text{X}}$	ΔT^{X}	$\Delta V_{\text{ne}}^{\text{XX}}$	$\Delta V_{\text{ee}}^{\text{XX}}$	$q_{\text{free}}^{\text{X}}$	$q_{\text{L}_{\text{p-org}}}^{\text{X}}$	ΔE^{X}	ΔN^{X}	ΔVol^{X}	$\Delta d_{\text{e}}^{\text{X}}$
						NTPA						
αC	–3.5	0.1	–3.6	–2.2	–16.1	14.7	0.343	0.332	7.4	0.011	0.43	–0.0008
αH–1	0.2	1.2	–1.0	6.2	–13.3	6.0	–0.002	–0.029	–6.2	0.027	2.02	–0.0004
αH–2	0.3	0.7	–0.5	7.8	–15.4	7.1	–0.014	–0.044	–8.0	0.030	1.99	–0.0003
βC	–1.4	–0.3	–1.1	–3.9	9.4	–6.6	0.006	0.007	10.2	–0.002	0.86	–0.0015
βH-1	1.1	–1.1	2.2	–2.1	4.4	0.0	–0.005	0.002	2.5	–0.007	–2.89	0.0011
βH-2	–0.2	2.1	–2.3	3.5	–9.7	3.9	–0.010	–0.032	–2.8	0.022	4.49	–0.0015
γC	–46.1	–24.6	–21.5	21.5	–107.9	64.9	1.619	1.578	–18.3	0.041	1.56	–0.0036
O(nb)	38.3	0.7	37.7	75.5	–298.9	261.1	–1.298	–1.375	–64.6	0.077	3.82	–0.0009
O(b)	56.1	73.8	–17.8	–58.7	380.7	–339.7	–1.298	–1.169	76.1	–0.129	–21.24	0.0084
N	20.8	50.5	–29.7	–56.3	465.2	–438.6	–1.020	–0.813	72.0	–0.207	–25.45	0.0363
						NTA						
αC	–1.5	2.1	–3.6	–16.1	38.3	–25.8	0.313	0.322	23.0	–0.009	2.67	–0.0056
αH-1	0.2	2.8	–2.6	3.8	–11.0	4.5	0.019	–0.006	–3.6	0.025	4.22	–0.0014
αH-2	–0.3	0.6	–0.9	4.8	–7.3	1.7	–0.027	–0.034	–5.0	0.007	0.70	–0.0002
βC	–17.0	2.0	–19.0	23.9	–105.5	62.7	1.630	1.588	–21.7	0.042	2.04	–0.0049
O(nb)	18.7	–19.7	38.4	81.4	–291.7	248.7	–1.305	–1.369	–73.1	0.064	2.44	–0.0005
O(b)	29.2	56.7	–27.5	–72.5	362.3	–317.3	–1.291	–1.193	87.3	–0.098	–9.13	0.0032
N	5.0	9.9	–4.9	–21.4	181.9	–165.4	–1.019	–0.926	31.2	–0.093	–17.55	0.0268

[a] $E_{\text{self}}^{\text{X}} = T^{\text{X}} + V_{\text{ne}}^{\text{XX}} + V_{\text{ee}}^{\text{XX}}$, by definition; T^{X} - the electronic kinetic energy of an atom (a Hamiltonian form); $V_{\text{ne}}^{\text{XX}}$ - attraction energy between electron density distribution of atom X and nucleus of Atom X; $V_{\text{ee}}^{\text{XX}}$ - two-electron interaction energy of atom X with itself; E^{X} - approximation to a virial-based total energy of atom X; N^{X} - average No of electrons in atom X (atomic electron population); Vol^{X} – atomic volume in bohr^3 (volume bounded by interatomic surfaces of atom X and by isosurface of the electron density distribution (0.001au isodensity surface was used); $d_{\text{e}}^{\text{X}} = N(Vol^{\text{X}})/Vol^{\text{X}}$ - average electron density in Vol^{X} where $N(Vol^{\text{X}})$ is average number of electrons in Vol^{X}.

The analysis of energy components, an intra-atomic contribution ($\Delta E_{\text{self}}^{\text{X}}$) and interatomic contributions ($0.5\sum_{\text{Y}\neq\text{X}}\Delta E_{\text{int}}^{\text{X,Y}}$) which, when summed up result in $\Delta E_{\text{add}}^{\text{X}}$ as shown in Eq. (S8), in combination with additional physical properties shown in Table 3, lead to the following conclusions:

(i) For the negatively charged atoms involved in contacts in $\mathcal{L}_{\text{p}}$, O(b) and N, the energy penalty is driven by destabilizing change in interactions with all remaining atoms in a ligand which is much greater in value than the change in their self-atomic energies; $0.5\sum_{\text{Y}\neq\text{X}}\Delta E_{\text{int}}^{\text{X,Y}} >> \left|\Delta E_{\text{self}}^{\text{X}}\right|$. The process of preorganization forced a large outflow of electron density from the negatively charged atoms, *e.g.*, ΔN^{N} = –0.207 and –0.093*e* for NTPA and NTA, respectively, which is accompanied by the most significant among all atoms contraction in atomic volume, *e.g.*, ΔVol^{N} = –25.4 and –17.5 bohr^3 for NTPA and NTA, respectively; note that these changes are more significant for NTPA. Because of that, a reduction in the electron-electron repulsion, $\Delta V_{\text{ee}}^{\text{X,X}} < 0$, and the electron-neutron attraction, $\Delta V_{\text{ne}}^{\text{X,X}} > 0$, within atomic basins is observed (note that one always observes $\Delta V_{\text{ne}}^{\text{X,X}} > \left|\Delta V_{\text{ee}}^{\text{X,X}}\right|$ for the O(b) and N atoms in both ligands). These two changes, in combination with $\Delta T^{\text{X}} < 0$, explain the observed decrease in these atoms self-energy, $\Delta E_{\text{self}}^{\text{X}} < 0$; recall that $E_{\text{self}}^{\text{X}} = T^{\text{X}} + V_{\text{ne}}^{\text{X,X}} + V_{\text{ee}}^{\text{X,X}}$.

(ii) For the oxygen atoms not bonded to the central metal ion, O(nb) of the carboxylate groups, the opposite is noted: the origin of the observed increase of these atoms additive atomic energies can be traced to unfavourable increase in their self-atomic energies resulting in $0.5\sum_{\text{Y}\neq\text{X}}\Delta E_{\text{int}}^{\text{X,Y}} << \Delta E_{\text{self}}^{\text{X}}$. It is also clear that to accommodate the dissipation of electron density from the crowded coordination sphere region in $\mathcal{L}_{\text{p}}$, a large inflow of electron density into negatively charged O(nb) atoms took place, $\Delta N^{\text{O(nb)}}$ = 0.077*e*, and this increased these atoms volume, $\Delta Vol^{\text{O(nb)}}$ = 3.8 bor^3. Interestingly, this was accompanied by a small decrease in the average electron density per unit volume, $\Delta d_{\text{e}}^{\text{O(nb)}} < 0$. As a consequence, the electron-electron repulsion, $\Delta V_{\text{ne}}^{\text{X,X}} > 0$, as well as electron-neutron attraction, $\Delta V_{\text{ne}}^{\text{X,X}} < 0$, increased in these atoms basins. Here, despite

$\left|\Delta V_{\mathrm{ne}}^{\mathrm{X,X}}\right| > \left|\Delta V_{\mathrm{ee}}^{\mathrm{X,X}}\right|$, we see that $\Delta T^{\mathrm{X}} > \left|\Delta V_{\mathrm{ne}}^{\mathrm{XX}} + \Delta V_{\mathrm{ee}}^{\mathrm{XX}}\right|$ and this fully explains the observed large increase in self-atomic energies found for O(nb).

(iii) Considering the highly, positively charged C-atoms of the carboxylate groups, the preorganization process resulted in increased stability of these atoms, $\Delta E_{\mathrm{add}}^{\mathrm{X}} << 0$, mainly due to a decrease in their self-atomic energies, $\Delta E_{\mathrm{self}}^{\mathrm{X}} < 0$. Interestingly, the γC-atoms of NTPA found themselves in more attractive molecular environment as judged from the highly stabilizing change in these atoms interactions with remaining atoms of the ligand, $0.5\sum_{\mathrm{Y}\neq\mathrm{X}}\Delta E_{\mathrm{int}}^{\mathrm{X,Y}}$ = –24.6 kcal/mol, but only a small, although unfavourable, change in diatomic interactions with remaining atoms is observed for the βC-atoms of NTA. From the observed $\Delta N^{\mathrm{X}} > 0$ (the charge decreases from 1.619 to 1.578), it also follows that electron population increased not only in highly negatively charged atoms, which are not directly involved in the steric contacts in the $\mathcal{L}_{\mathrm{p}}$ form of the ligands, but also for highly and positively charged C-atoms of the carboxylic groups. This means that all highly charged (negatively and positively) atoms which are in close proximity to the centre of the coordination sphere experienced an increase in the electron density which clearly facilitates the charge dissipation and must have resulted in somewhat smaller repulsive nature of diatomic interactions between atoms in the coordination sphere.

In general, except for a difference in the sign and value of the interaction energies with remaining atoms, all other physical properties of the C-atoms of the carboxylic groups are characterized by comparable in value and of the same sign changes observed when going from the $\mathcal{L}_{\mathrm{f}}$ to $\mathcal{L}_{\mathrm{p}}$ state of the ligands.

Another striking observation can be made, namely the additive atomic energies of all H-atoms, regardless whether they were/are involved in close contacts (αH-1 and βH-1) in $\mathcal{L}_{\mathrm{f}}/\mathcal{L}_{\mathrm{p}}$ have not changed significantly, typically by a fraction of kcal/mol. Also, their self-atomic energies changed marginally. This observation contradicts again the common notion that H-atoms involved in a steric clash become highly strained; clearly this is not the case for these two ligands.

In summary, the energy penalty experienced on preorganization is due to a global unfavourable change in all diatomic interactions with O(b) and N atoms playing the most significant role. Importantly, to minimize the intra-coordination-sphere strain, electron density has been dissipated and this resulted in (i) the destabilization of the O(nb) atoms, (ii) stabilization of the C-atoms in the carboxylate groups, and (iii) formation of AILs between donor atoms. The difference in the preorganization strain energy, between NTPA and NTA, is largely due to the formation of far more repulsive interactions in NTPA as measured by $0.5\sum_{Y \neq X} \Delta E_{\text{int}}^{X,Y}$. Contrary to classical suggestions, our findings show that the H-atoms involved in short contacts (and the same applies to all H-atoms of the ligands) play a negligible role when they contribution to the preorganization energy is considered.

3.2.2. Exploring Binding Stage of Complex Formation

Hypothetically, there are four possibile scenarios, when a metal ion $\mathscr{M}$ spontaneously forms two complexes with two ligands, ML(1) and ML(2), which lead to the preferential formation of ML(1):

1. $E_{\text{p-org}}^{\text{ML(1)}} < E_{\text{p-org}}^{\text{ML(2)}}$ and $\left|E_{\text{bind}}^{\text{ML(1)}}\right| < \left|E_{\text{bind}}^{\text{ML(1)}}\right|$, but $\left|E_{\text{p-org}}^{\text{ML(1)}} + E_{\text{bind}}^{\text{ML(1)}}\right| > \left|E_{\text{p-org}}^{\text{ML(2)}} + E_{\text{bind}}^{\text{ML(2)}}\right|$,
2. $E_{\text{p-org}}^{\text{ML(1)}} < E_{\text{p-org}}^{\text{ML(2)}}$ but $\left|E_{\text{bind}}^{\text{ML(1)}}\right| > \left|E_{\text{bind}}^{\text{ML(1)}}\right|$,
3. $E_{\text{p-org}}^{\text{ML(1)}} > E_{\text{p-org}}^{\text{ML(2)}}$, $\left|E_{\text{bind}}^{\text{ML(1)}}\right| < \left|E_{\text{bind}}^{\text{ML(1)}}\right|$, but still $\left|E_{\text{p-org}}^{\text{ML(1)}} + E_{\text{bind}}^{\text{ML(1)}}\right| > \left|E_{\text{p-org}}^{\text{ML(2)}} + E_{\text{bind}}^{\text{ML(2)}}\right|$, and
4. $E_{\text{p-org}}^{\text{ML(1)}} > E_{\text{p-org}}^{\text{ML(2)}}$ and $\left|E_{\text{bind}}^{\text{ML(1)}}\right| > \left|E_{\text{bind}}^{\text{ML(1)}}\right|$ but $\left|E_{\text{p-org}}^{\text{ML(1)}} + E_{\text{bind}}^{\text{ML(1)}}\right| > \left|E_{\text{p-org}}^{\text{ML(2)}} + E_{\text{bind}}^{\text{ML(2)}}\right|$.

Considering our case, where L(1) = NTPA and L(2) = NTA, we are dealing with the case 4 of the above scenario because $E_{\text{p-org}}^{\text{BeNTPA}} > E_{\text{p-org}}^{\text{BeNTA}}$, $\left|E_{\text{bind}}^{\text{ML(1)}}\right| > \left|E_{\text{bind}}^{\text{ML(1)}}\right|$ but the overall energy result is $\left|E_{\text{p-org}}^{\text{ML(1)}} + E_{\text{bind}}^{\text{ML(1)}}\right| > \left|E_{\text{p-org}}^{\text{ML(2)}} + E_{\text{bind}}^{\text{ML(2)}}\right|$. This clearly shows that knowledge of binding energy is informative but does not point directly at the more stable complex on one hand and does not provide any insight on mechanisms or origin of energetic changes leading to the preferential complex formation on the other hand. Hence, we decided to decompose the computed E_{bind} by making use of the primary and molecular fragment energy terms expressed within the IQA/IQF framework. The concept of fragment energies can be traced back to ideas coming from the theory of electronic separability of McWeeny,[86] but they were not used extensively. What follows is a new implementation of these ideas to investigate relative stability of molecules/metal complexes or, in general, molecular systems.

According to the IQF framework,[68,87] the energy of a molecular system is defined as

$$E = \sum_{\mathcal{F}} E_{\text{intra}}^{\mathcal{F}} + 0.5 \sum_{\mathcal{F}} \sum_{\mathcal{G} \neq \mathcal{F}} E_{\text{int}}^{\mathcal{F},\mathcal{G}} \tag{3}$$

Recall that the binding energy is defined as, $E_{\text{bind}} = E(\text{BeL}) - E(\mathcal{L}_{\text{p}}) - E(\mathcal{M}_{\text{f}})$. To gain further insight, one can decompose the binding energy into IQF-defined components:

$$E_{\text{bind}} = E_{\text{intra}}^{\mathcal{L}_{\text{c}}} + E_{\text{intra}}^{\mathcal{M}_{\text{c}}} + E_{\text{int}}^{\mathcal{L}_{\text{c}},\mathcal{M}_{\text{c}}} - E_{\text{intra}}^{\mathcal{L}_{\text{p}}} - E_{\text{intra}}^{\mathcal{M}_{\text{f}}} \tag{4}$$

The first two terms in Eq. 4 represent the intra-fragment energy which can defined as the sum of the self-atomic energies of all atoms and diatomic interaction energies between the atoms within in each fragment; the third term is the interaction energy between the two fragments, $\mathcal{M}_{\text{c}}$ and $\mathcal{L}_{\text{c}}$; the fourth term and fifth terms account for the intra-fragment energies of $\mathcal{L}_{\text{p}}$ and $\mathcal{M}_{\text{f}}$. Note that $\mathcal{M}_{\text{f}}$ and $\mathcal{M}_{\text{c}}$ are monoatomic fragments, hence $E_{\text{intra}}^{\mathcal{M}_{\text{f}}} = E_{\text{self}}^{\mathcal{M}_{\text{f}}}$ and $E_{\text{intra}}^{\mathcal{M}_{\text{c}}} = E_{\text{self}}^{\mathcal{M}_{\text{c}}}$. We can hence define the deformation energy of each fragment as being the change in the intra-fragment energy of each fragment. For the ligand fragment it would be defined as:

$$E_{\text{def}}^{\mathcal{L}} = E_{\text{intra}}^{\mathcal{L}_{\text{c}}} - E_{\text{intra}}^{\mathcal{L}_{\text{p}}} \tag{5}$$

And for the metal fragment it would be:

$$E_{\text{def}}^{\mathcal{M}} = E_{\text{self}}^{\mathcal{M}_{\text{c}}} - E_{\text{self}}^{\mathcal{M}_{\text{f}}} \tag{6}$$

And hence the binding energy can be re-written as:

$$E_{\text{bind}} = E_{\text{def}}^{\mathcal{L}} + E_{\text{def}}^{\mathcal{M}} + E_{\text{int}}^{\mathcal{L}_{\text{c}},\mathcal{M}_{\text{c}}} \tag{7}$$

By definition, the intra-fragment energy of $\mathcal{L}_{\text{p}}$ is:

$$E_{\text{intra}}^{\mathcal{L}_{\text{p}}} = \sum_{\text{X} \in \mathcal{L}_{\text{p}}} E_{\text{self}}^{\text{X}} + 0.5 \sum_{\text{X} \in \mathcal{L}_{\text{p}}} \sum_{\substack{\text{X} \neq \text{Y} \\ \text{Y} \in \mathcal{L}_{\text{p}}}} E_{\text{int}}^{\text{X,Y}} \tag{8}$$

and that for $\mathcal{L}_{\text{c}}$ is:

$$E_{\text{intra}}^{\mathcal{L}_{\text{c}}} = \sum_{\text{X} \in \mathcal{L}_{\text{c}}} E_{\text{self}}^{\text{X}} + 0.5 \sum_{\text{X} \in \mathcal{L}_{\text{c}}} \sum_{\substack{\text{X} \neq \text{Y} \\ \text{Y} \in \mathcal{L}_{\text{c}}}} E_{\text{int}}^{\text{X,Y}} \tag{9}$$

To account for the total energy contribution coming from the self-atomic energies of all atoms when the pre-organized ligand and a free metal ion bind to form a final complex ML, one can combine relevant energy terms

$$\Delta E_{\mathrm{self}}^{\mathrm{ML}} = \sum_{\mathrm{X}\in\mathrm{ML}} \Delta E_{\mathrm{self}}^{\mathrm{X}} = \sum_{\mathrm{X}\in\mathcal{L}_{\mathrm{c}}} E_{\mathrm{self}}^{\mathrm{X}} + E_{\mathrm{self}}^{\mathcal{M}_{\mathrm{c}}} - \sum_{\mathrm{X}\in\mathcal{L}_{\mathrm{p}}} E_{\mathrm{self}}^{\mathrm{X}} - E_{\mathrm{self}}^{\mathcal{M}_{\mathrm{f}}} \tag{10}$$

where $\Delta E_{\mathrm{self}}^{\mathrm{ML}}$ stands for a change in the molecular system self-energy.

Because there are two fragments in the molecular system investigated here, a polyatomic $\mathcal{L}$ and monoatomic $\mathcal{M}$, the total energy contribution attributed to the combined change in self-energies of all atoms in a complex, $\Delta E_{\mathrm{self}}^{\mathrm{ML}}$, can be conveniently divided into those for each atom of the ligand, $\Delta E_{\mathrm{self}}^{\mathcal{L}}$, when it changes from the $\mathcal{L}_{\mathrm{p}}$ to $\mathcal{L}_{\mathrm{c}}$ state and $\Delta E_{\mathrm{self}}^{\mathcal{M}}$, when the free metal ion $\mathcal{M}_{\mathrm{f}}$, changes to its state in the complex, $\mathcal{M}_{\mathrm{c}}$, which is effectively $E_{\mathrm{def}}^{\mathcal{M}}$.

$$\Delta E_{\mathrm{self}}^{\mathrm{ML}} = E_{\mathrm{def}}^{\mathcal{M}} + \Delta E_{\mathrm{self}}^{\mathcal{L}} \tag{11}$$

where

$$\Delta E_{\mathrm{self}}^{\mathcal{L}} = \sum_{\mathrm{X}\in\mathcal{L}_{\mathrm{c}}} E_{\mathrm{self}}^{\mathrm{X}} - \sum_{\mathrm{X}\in\mathcal{L}_{\mathrm{p}}} E_{\mathrm{self}}^{\mathrm{X}} \tag{12}$$

A new term, $\Delta E_{\mathrm{int}}^{\mathcal{L}}$, can be recovered that estimates an energy gain/loss caused just by the changes in all unique diatomic intra-ligand interaction energies when the ligand changed its state from being preorganized, $\mathcal{L}_{\mathrm{p}}$ state, to that in the complex, $\mathcal{L}_{\mathrm{c}}$ state,

$$\Delta E_{\mathrm{int}}^{\mathcal{L}} = 0.5 \sum_{\mathrm{X}\in\mathcal{L}_{\mathrm{c}}} \sum_{\substack{\mathrm{X}\neq\mathrm{Y}\\ \mathrm{Y}\in\mathcal{L}_{\mathrm{c}}}} E_{\mathrm{int}}^{\mathrm{X,Y}} - 0.5 \sum_{\mathrm{X}\in\mathcal{L}_{\mathrm{p}}} \sum_{\substack{\mathrm{X}\neq\mathrm{Y}\\ \mathrm{Y}\in\mathcal{L}_{\mathrm{p}}}} E_{\mathrm{int}}^{\mathrm{X,Y}} \tag{13}$$

The interaction energy between the two fragments is the sum of all unique interactions between the atoms of $\mathcal{L}_{\mathrm{c}}$ and $\mathcal{M}_{\mathrm{c}}$.

$$E_{\mathrm{int}}^{\mathcal{L}_{\mathrm{c}},\mathcal{M}_{\mathrm{c}}} = \sum_{\mathrm{X}\in\mathcal{M}_{\mathrm{c}}} \sum_{\mathrm{Y}\in\mathcal{L}_{\mathrm{c}}} E_{\mathrm{int}}^{\mathrm{X,Y}} = \sum_{\substack{\mathrm{X}\neq\mathcal{M}_{\mathrm{c}}\\ \mathrm{X}\in\mathrm{ML}}} V_{\mathrm{int}}^{\mathcal{M}_{\mathrm{c}},\mathrm{X}} \tag{14}$$

It is important to note that this step expands our analysis from a focus on just coordination bonds to scrutinizing all possible interactions involving complexed metal ion, $\mathcal{M}_{\mathrm{c}}$.

By making use of expression 4, 10 and 13, we can express binding energy (Eq. 2) as

$$E_{\mathrm{bind}} = \Delta E_{\mathrm{self}}^{\mathrm{ML}} + \Delta E_{\mathrm{int}}^{\mathcal{L}} + E_{\mathrm{int}}^{\mathcal{L}_{\mathrm{c}},\mathcal{M}_{\mathrm{c}}} \tag{15}$$

which accounts for the global changes in self-atomic energy of a molecular system as well as, variation in the intra-ligand and inter-fragment interactions.

To gain deeper insight on the origin of E_{bind}, one can determine classical and XC contributions making up the inter-fragment interaction energy $E_{\mathrm{int}}^{\mathcal{M}_\mathrm{c},\mathcal{L}_\mathrm{c}}$ term and this can be easily computed from

$$E_{\mathrm{int}}^{\mathcal{M}_\mathrm{c},\mathcal{L}_\mathrm{c}} = V_{\mathrm{cl}}^{\mathcal{M}_\mathrm{c},\mathcal{L}_\mathrm{c}} + V_{\mathrm{XC}}^{\mathcal{M}_\mathrm{c},\mathcal{L}_\mathrm{c}} = \sum_{\substack{\mathrm{X}\neq\mathcal{M}_\mathrm{c} \\ \mathrm{X}\in\mathrm{ML}}} V_{\mathrm{cl}}^{\mathcal{M}_\mathrm{c},\mathrm{X}} + \sum_{\substack{\mathrm{X}\neq\mathcal{M}_\mathrm{c} \\ \mathrm{X}\in\mathrm{ML}}} V_{\mathrm{XC}}^{\mathcal{M}_\mathrm{c},\mathrm{X}} . \tag{16}$$

The important difference between Eq. 15 and 7 is in that the contributions coming from intra-atomic energies, $\Delta E_{\mathrm{self}}^{\mathrm{ML}}$, and diatomic interactions within a particular fragment, $\Delta E_{\mathrm{int}}^{\mathcal{L}}$, are expressed in terms of relevant deformation energy terms, which, as will be seen from discussion that follows, will be of great help in tracking the origin and nature of factors controlling preferential affinity between two fragments, $\mathcal{M}$ and $\mathcal{L}$, in both complexes making the interpretation of relevant stability of molecular systems much easier and more convincing.

A set of energy terms used to understand and interpret binding energies of the two complexes, BeNTA and BeNTPA, is included in Table 4. It conclusively points at BeNTPA as preferentially formed because ΔE_{bind} = –8.5 kcal/mol was found to be in favour of this complex. As expected, due to the limitations of the AIMAll software, we have not obtained the exact value of ΔE_{bind} determined form electronic energies, but we have recovered the trend and it is clear that it is driven by the inter-fragment interaction energy term, $E_{\mathrm{int}}^{\mathcal{M}_\mathrm{c},\mathcal{L}_\mathrm{c}}$. This exemplifies the importance and significance of the protocol proposed in this work. Note that using just the sum of interaction energies of all coordination bonds (hence their strength) as a predictive tool pointed at BeNTA as more stable because this contribution was in favour of this complex by about 10 kcal/mol. However, through making use of the combined energy terms (molecular fragments' energies which account for all possible intra- and inter-fragment energy components) makes it clear that the additional interactions (excluding coordination bonds) contributed to the $E_{\mathrm{int}}^{\mathcal{M}_\mathrm{c},\mathcal{L}_\mathrm{c}}$ energy term which was found here to be responsible for higher stability of the BeNTPA complex. Furthermore, these results clearly demonstrate that formation of a chemical bond (here coordination bonds) in a multi-atomic environment is not an affair localized to M—L interatomic region but it must be viewed as a global, on a molecular scale, event. Importantly, the computed binding energies also agree with chemists' intuition as the recovered trend – the larger interaction energy between free metal ion and an incoming ligand (and the resultant binding energy), the stronger complex is formed – is exactly what one would expect.

Table 4. The indicated energy components (in kcal/mol), computed within a IQA/IQF framework, which were used in the interpretation of relative stability of BeNTA and BeNTPA complexes. Selected MP2 data is shown in brackets.

Energy term	BeNTA	BeNTPA	ΔE[a]
Energy components of E_{bind}			
$E_{\text{def}}^{\mathcal{M}}$	–123.4 (–134.1)	–122.6 (–133.3)	0.8 (0.8)
$E_{\text{def}}^{\mathcal{L}}$	119.7	132.3	12.5
$E_{\text{int}}^{\mathcal{M}_c,\mathcal{L}_c}$	–1043.5 (–1064.9)	–1065.4 (–1088.5)	–21.9 (–23.6)
E_{bind}	–1047.2	–1055.7	–8.5
Additional energy terms			
$\Delta E_{\text{self}}^{\text{ML}}$	112.5	126.2	13.7
$\Delta E_{\text{int}}^{\mathcal{L}}$	–116.2	–116.5	–0.3
$V_{\text{cl}}^{\mathcal{M}_c,\mathcal{L}_c}$	–941.41	–964.4	–23.0
$V_{\text{XC}}^{\mathcal{M}_c,\mathcal{L}_c}$	–102.1	–101.0	1.1

[a] $\Delta E = E(\text{NTPA}) - E(\text{NTA})$

From the binding energy perspective it is evident that Be has large affinity to both ligands as, in absolute value, this energy term is above one thousand kcal/mol. Moreover, the change from the free to the complexed metal ion stabilized Be. As a result, $E_{\text{def}}^{\mathcal{M}}$ is also stabilizing in both complexes with no significant difference between the two complexes; thus from this perspective the metal ion does not show a preference toward a 5- or 6-membered coordination rings.

Looking now from the ligand perspective we note that the deformation energy, $E_{\text{def}}^{\mathcal{L}}$, of NTPA is larger by about 12 kcal/mol even though BeNTA consistently shows more significant deviations from the minimum strain energy geometries (Table S5 in Supplementary Information).

From the analysis of additional energy terms shown in Table 4 it follows that a significant increase in the self-energy of the atoms is observed on both complex formation even though the pre-organized ligands were used as an initial state. Furthermore, the total change in self-energy of molecular systems (here beryllium complexes) $\Delta E_{\text{self}}^{\text{ML}}$, is larger by about 13.7 kcal/mol for BeNTPA (most likely because there are more atoms in BeNTPA). However, $\Delta E_{\text{self}}^{\text{ML}}$ is compensated over by highly favourable change in the interaction energies between Be and the remaining atoms of $\mathcal{L}$. These inter-fragment interactions are highly dominated by classical (electrostatic) term and we observe $V_{\text{cl}}^{\mathcal{M}_{\text{c}},\mathcal{L}_{\text{c}}}$ (i) an order of magnitude larger than the $V_{\text{XC}}^{\mathcal{M}_{\text{c}},\mathcal{L}_{\text{c}}}$ term for both complexes, and (ii) more significant, by –23 kcal/mol, in BeNTPA. Furthermore, it is clear that the classical term of inter-fragment interaction energy has contributed the most to higher stability of BeNTPA because the exchange-correlation terms in both complexes are very much of the same value, about –100 kcal/mol, which still should be seen as significant contribution of covalent nature. As one would expect, the overall change in the interaction energies between atoms of a ligand, the intra-fragment interaction energy term, $\Delta E_{\text{int}}^{\mathcal{L}}$, is of highly stabilizing.

Origin of different binding energies. The above fragment-based analysis allowed us to identify the main source of higher BeNTPA stability, the inter-fragment interaction energy. Hence, we decided to analyse individual components of $E_{\text{int}}^{\mathcal{M}_{\text{c}},\mathcal{L}_{\text{c}}}$ with an aim of finding the origin of the resultant effect - see relevant data in Table 5. The analysis of data shown in Table 5 leads to a number of interesting and important observation:

(a) The XC term is only significant in the case of coordination bonds which is in agreement with common sense and chemists' intuition,

(b) Interactions of Be with electronegative atoms (oxygen and nitrogen) are attractive whereas all other interactions are electrostatically repulsive,

(c) There is a clear trend in the repulsive energies involving C-atoms and Be in both complexes; interactions involving C-atoms of carboxylate groups are about 4.5 times larger when compared with α-carbons. Note also that interactions with β-carbons in BeNTPA are order(s) of magnitude smaller.

(d) Interactions between Be and O(nb)- and N-atoms are more attractive, by about –4 and –14 kcal/mol, respectively, in BeNTA (the interaction energies with O(b) are comparable in both complexes).

(e) The sum of all attractive Be-X interactions (where X = N, O(nb) and O(b)) accounts for –2473.6 and –2451.8 kcal/mol in BeNTA and BeNTPA, respectively (a difference of about 22 kcal/mol in favour of BeNTA).

(f) The sum of all repulsive interactions, however, is greater in BeNTA than in BeNTPA (1430.1 and 1386.5 kcal/mol, respectively); a difference of about 44 kcal/mol in favour of BeNTPA despite the presence of additional atoms with which the beryllium has repulsive interactions in this complex.

Table 5. IQA partitioning of two-bodied interaction energies of all interactions with the Be atom in BeNTPA and BeNTA using the RXL3YP wavefunction on the MP2 structures.

BeNTPA					BeNTA				
Atoms X	Y	$V_{\mathrm{cl}}^{\mathrm{X,Y}}$	$V_{\mathrm{XC}}^{\mathrm{X,Y}}$	$E_{\mathrm{int}}^{\mathrm{X,Y}}$	Atoms X	Y	$V_{\mathrm{cl}}^{\mathrm{X,Y}}$	$V_{\mathrm{XC}}^{\mathrm{X,Y}}$	$E_{\mathrm{int}}^{\mathrm{X,Y}}$
Be	αC	79.0	–0.2	78.8	Be	αC	83.0	–0.2	82.8
Be	αH–1	7.6	0.0	7.6	Be	αH–1	14.6	0.0	14.6
Be	αH–2	7.7	–0.1	7.6	Be	αH–2	13.1	0.0	13.1
Be	αC	79.1	–0.2	78.9	Be	αC	83.2	–0.2	83.0
Be	αH–1	7.5	0.0	7.5	Be	αH–1	14.6	0.0	14.6
Be	αH–2	7.7	–0.1	7.6	Be	αH–2	13.1	0.0	13.1
Be	αC	79.1	–0.2	78.9	Be	αC	83.2	–0.2	83.0
Be	αH–1	7.6	0.0	7.6	Be	αH–1	14.6	0.0	14.6
Be	αH–2	7.7	–0.1	7.6	Be	αH–2	13.2	0.0	13.1
Be	βC	3.6	–0.1	3.5	Be	βC	366.5	–0.3	366.1
Be	βH–1	8.4	0.0	8.4	Be	O(nb)	–194.3	–0.2	–194.5
Be	βH–2	7.2	0.0	7.2	Be	O(b)	–457.6	–26.7	–484.4
Be	βC	3.6	–0.1	3.5	Be	βC	366.5	–0.3	366.2
Be	βH–1	8.4	0.0	8.4	Be	O(nb)	–194.3	–0.2	–194.5
Be	βH–2	7.2	0.0	7.2	Be	O(b)	–457.6	–26.7	–484.3
Be	βC	3.6	–0.1	3.5	Be	βC	366.3	–0.3	366.0
Be	βH–1	8.4	0.0	8.4	Be	O(nb)	–194.2	–0.2	–194.4
Be	βH–2	7.3	0.0	7.2	Be	O(b)	–457.6	–26.8	–484.3
Be	γC	349.3	–0.3	349.0	Be	N	–417.8	–19.4	–437.2
Be	O(nb)	–190.7	–0.2	–190.9	Sum (kcal/mol):		**–941.4**	**–102.1**	**–1043.5**
Be	O(b)	–459.0	–25.9	–484.9					
Be	γC	349.2	–0.3	348.9					
Be	O(nb)	–190.7	–0.2	–190.9					
Be	O(b)	–458.9	–26.0	–484.9					
Be	γC	349.3	–0.3	349.1					
Be	O(nb)	–190.7	–0.2	–190.9					
Be	O(b)	–459.0	–25.9	–484.9					
Be	N	–403.8	–20.5	–424.3					
Sum (kcal/mol):		**–964.4**	**–101.0**	**–1065.4**					

The above analysis leads to quite an unexpected conclusion that, in terms of interaction energies, this is not the strength of coordination bonds that controls the relative stability of these complexes but the unfavourable interactions which are significantly less severe in the case of BeNTPA. Frenking *et al*.[88,89] reach a similar conclusion, indicating that the strength of metal complexes is not necessarily dependent on the metal-ligand bonds but rather the total interaction of the metal to the ligand fragment.

Finally, the presence of the inductive effect can also be deduced here; the repulsion between the beryllium ion and the α-carbon atoms is approximately 4.0 kcal/mol greater in BeNTA than in BeNTPA and the repulsion with the carboxylate carbon atoms is ~17 kcal/mol greater. It is also interesting to note that there is significant and measurable repulsion with α-hydrogens which is almost twice as large in BeNTA.

Table 6. Relative to $\mathcal{L}_p$ and $\mathcal{M}_f$ structures, changes in the selected QTAIM properties of atoms in BeNTPA and BeNTA complexes.

Atom X	$q^{X}_{p\text{-org}}$	q^{X}_{comp}	ΔN^{X}
BeNTPA			
αC	0.332	0.302	0.030
αH–1	–0.029	0.033	–0.061
αH–2	–0.044	0.032	–0.076
βC	0.007	–0.009	0.016
βH–1	0.002	0.037	–0.035
βH–2	–0.032	0.042	–0.074
γC	1.578	1.618	–0.040
O(nb)	–1.375	–1.231	–0.145
O(b)	–1.169	–1.352	0.183
N	–0.813	–1.148	0.336
Be	2.000	1.729	0.271
BeNTA			
αC	0.322	0.290	0.032
αH-1	–0.006	0.066	–0.072
αH-2	–0.034	0.061	–0.095
βC	1.588	1.635	–0.046
O(nb)	–1.369	–1.224	–0.145
O(b)	–1.193	–1.332	0.139
N	–0.926	–1.209	0.283
Be	2.000	1.723	0.277

A number of these IQF (Table 4) and IQA (Table 5) results can be explained by analysing QTAIM-defined net atomic charges and the changes in the electron populations – see Table 6. The stabilization of the $\mathcal{M}$ fragment ($E^{\mathcal{M}}_{def}$ < 0) can be explained by the donation of density to the bare metal ion by the ligand (as measured by an increase in electron population, $\Delta N^{\mathcal{M}} > 0$) resulting in a less positive charge. The converse change in the $\mathcal{L}$ fragment ($E^{\mathcal{L}}_{def} > 0$) can be explained by the decrease in the electron population ($\Delta N^{\mathcal{L}} < 0$). $\Delta N^{\mathcal{L}}$ for both complexes is comparable (–0.277 and –0.271 au in BeNTA and BeNTPA respectively) but the change is distributed amoungest all atoms in the $\mathcal{L}$ fragment, resulting in the final charges in the complex, $q^{\mathrm{X}}_{\mathrm{comp}}$, as shown Table 6. Recall that the binding energy is controlled by the interaction between two fragments, $E^{\mathcal{M}_c,\mathcal{L}_c}_{\mathrm{int}}$, and the dominant factor is the classical term (–21.9 kcal/mol in favour of BeNTPA) and the exchange-correlation term is comparable between the two complexes. Also, the preferential binding in BeNTPA is due to the less severe repulsive interactions of $\mathrm{Be^{II}}$ metal centre with the backbone of the ligand. These differences in the interactions can be explained using the resultant charges on the atoms in the complexes. αH-atoms are less positively charged in BeNTPA (*e.g.* $q^{\alpha\mathrm{H\text{-}1}}_{\mathrm{comp}}$ is 0.033 and 0.066 in BeNTPA and BeNTA respectively), as well as the C-atoms of the carboxylate groups ($q^{\mathrm{X}}_{\mathrm{comp}}$ is 1.618 and 1.635 au in BeNTPA and BeNTA respectively). This results in a smaller charge difference between these atoms and the Be atom. This observation, in conjunction with the greater interatomic distances in BeNTPA (because it has a larger chelate ring with more atoms), results in the electrostatic term of the individual interactions in Table 5 being less repulsive in BeNTPA (*e.g.* $E^{\mathrm{Be},\alpha\mathrm{H\text{-}1}}_{\mathrm{int}}$ is approximately twice as large in BeNTA and the interaction with the carboxylate carbon being ~15 kcal/mol less repulsive in BeNTPA). The aggregate effect is that the classical term of the inter-fragment interaction energy is –23.0 kcal/mol more attractive in BeNTPA, and by extension the inter-fragment interaction energy and the binding energy.

Conclusions

The theoretical prediction of the relative stability of compounds (not only metal-containing species) is of paramount importance and a great effort has been made in, *e.g.*, predicting parameters controlling preferential formation of metal complexes in aqueous solutions.[1] This lead to a number of different simple and semi-empirical rules which were of great help in the ligand design strategies. The aim of this work was to fundamentally understand why beryllium forms a stronger complex with NTPA relative to NTA, whereas all other metal ions have larger formation constants with NTA. It is important to realize that our undertaking was not trivial and could be seen as ambitious because relative energy difference between the two complexes amounts to just 3.3 kcal/mol.

Following commonly used methodologies, we have examined numerous individual local indices (structural and topological) and a very mixed picture emerged; seven pointed at NTA and only four at NTPA as forming the stronger complex with Be. Furthermore, none of them were decisively in favour of a particular complex or large enough to override the significance of others. Those in favour of NTA were: (i) a shorter coordination Be–N bond, (ii) longer distance between 'clashing' H-atoms which then were found as not interacting by the NCI analysis (three such contacts were found in BeNTPA), (iii) on average larger density at BCPs of coordination bonds, (iv) larger density at RCPs, (v) larger (more negative) interaction energy between Be and N-atom, (vi) smaller repulsive interaction energy between O-atoms in the coordination sphere, and finally (vii) the sum of interaction energy of all coordination bonds. Considering descriptors pointing at BeNTPA: (i) slightly shorter (by 0.002 Å) Be–O coordination bonds and associated with that larger, by 0.004 a.u., density at BCPs, (ii) marginally more stabilizing, by –0.6 kcal/mol, interaction energy between Be and O-atoms of the coordination bonds, (iii) less repulsive interaction between N and O atoms of the coordination sphere, and also (iv) the sum of all repulsive interaction energies between donor atoms of the coordination sphere was smaller in the BeNTPA complex.

Although geometrical (structural), QTAIM-, IQA- or NCI-defined properties provided lots of information and interesting insights on numerous physical and fundamental properties of these complexes, none of the techniques was able to provide the sought after answer. It became very clear that a different approach was required. This inspired us to develop a methodology based on the concept of molecular fragments and their properties, rather than pursuing a classical approach focused on individual (or paired) atoms and their properties. We have also realized that much more information might be gained when changes in properties rather than properties in the final product (here a metal complex) are analysed on a fundamental level. To this effect we have implemented a simplified, two-stage process of complex formation; Stage 1 involved pre-organization of a ligand from the lowest energy structure to that observed in the complex whereas Stage 2 involved binding between free metal ion and the pre-organized ligand. Furthermore, two fragments were used in Stage 2, namely a monoatomic, $\mathscr{M}$, consisting of the central metal ion, here Be, and polyatomic $\mathscr{L}$ (a ligand) needed for fragment-based analyses.

An in depth QTAIM-and IQA-based analysis allowed us to uncover the origin and physical nature of larger strain computed for NTPA when it attained a pre-organized structure. In general, the larger penalty energy in NTPA was mainly due to the contribution made by all possible interactions between N- and O-donor atoms. Density was dissipated into the surrounding atoms upon preorganization which resulted in the large destabilization of O(b)- and O(nb)-atoms and stabilization of C-atoms of carboxylic groups. Importantly, we have also found that all H-atoms of the ligands (this also includes those involved in steric contacts) play a negligible role when the contribution to the preorganization energy is considered; typically, their additive energies changed by a fraction of kcal/mol, hence they were not (de)stabilized to any significant degree. To summarize this part, the computed difference in the pre-organization energy for both ligands showed that, as it was found also for larger metal ions, NTPA is more strained than NTA (hence there must be some other energy sources to reverse this trend and make BeNTPA more stable) but, importantly, we could point at the origin of the intramolecular strain in both ligands and this allowed us to find the main contributor on one hand and eliminate a major classic suspect, steric CH--HC contacts, on the other.

For the purpose of Stage 2 of complex formation (binding process between Be and pre-organized ligand) we derived an expression for the binding energy, $E_{\text{bind}} = E_{\text{def}}^{\mathcal{M}} + E_{\text{def}}^{\mathcal{L}} + E_{\text{int}}^{\mathcal{M}_c,\mathcal{L}_c}$, which is expressed in molecular fragments energy terms, deformation energies of metal and ligand fragments and inter-fragment interaction energy. The computed difference, ΔE_{bind}, fully recovered the experimentally observed relative stability of these two complexes. Furthermore, it became obvious that the energy source of higher stability of BeNTPA (i) is not related to coordination bonds (they were found stronger in BeNTA) but (ii) it comes from the overall more stabilizing contribution made by all possible interactions Be is involved in with all atoms of NTPA, the inter-fragment interaction energy term, $E_{\text{int}}^{\mathcal{M}_c,\mathcal{L}_c}$. The deformation energy, $E_{\text{def}}^{\mathcal{M}} = \Delta E_{\text{self}}^{\mathcal{M}}$, for a metal ion (it accounts for the change in self-atomic energy of Be on transition from the free to complexed state) has almost identical values in both complexes (the difference being within one kcal/mol). Deformation energy $E_{\text{def}}^{\mathcal{L}} = \Delta E_{\text{self}}^{\mathcal{L}} + \Delta E_{\text{int}}^{\mathcal{L}}$ for the ligands accounts for changes in all atoms self-energies and intra-fragment diatomic interactions of the ligand fragment $\mathcal{L}$; for both ligands we found $E_{\text{def}}^{\mathcal{L}} \geq +120$ kcal/mol with that for NTPA being ~12 kcal more significant. However, it was fully compensated over by the difference in the $E_{\text{int}}^{\mathcal{M}_c,\mathcal{L}_c}$ term which was found to be ~–22 kcal/mol more in favour of BeNTPA. Having established main source of higher BeNTPA stability we decided to search for its origin. The inspection of all intramolecular interactions Be is involved in both complexes revealed that all negatively charged atoms (N- and both O-atoms of carboxylic group) are involved in highly stabilizing interactions with Be whereas all remaining atoms are involved in repulsive interactions with Be, but overall they are by far less significant. Interestingly and somewhat unexpectedly, the total contribution made by attractive interactions was more significant in BeNTA by ~–22 kcal/mol. However, the sum of repulsive interaction was significantly smaller for BeNTPA by ~44 kcal/mol. Hence, the following picture emerged. The large attractive interactions between donor atoms and Be (they are in the range between –420 and –485 kcal/mol) can be seen as driving the complex formation to completion. Moreover, they are strongly assisted by interactions between Be and remaining O-atoms of carboxylic groups which are in the range between –190 and –195 kcal/mol in both complexes. The large energy released, more than –2500 kcal/mol, is partly compensated by positive (destabilizing) interactions and the larger compensation observed in BeNTA resulted in the more stable BeNTPA. This is an entirely unexpected, but highly informative, result as the relative stability of molecular systems does not have to be controlled by the strongest interactions (here coordination bonds). These results indicate a combined effect of other and much smaller in value energy sources which might decide on preferential formation of a system.

This is the first and, in our opinion, highly successful implementation of fragment-based interpretation of metal complexes relative stability, which must be seen as of general purpose. It is easy to imagine that the same protocol can be used in the study of, *e.g.*, preferential reaction path to predict most likely product of either organic or inorganic reaction, or preferential protonation site from which a protonation sequence could be predicted. An added value of the proposed protocol is gaining an invaluable insight (on a fundamental level) on the nature and origin of parameters controlling preferred formation of a compound.

ASSOCIATED CONTENT

Supporting Information.
All Cartesian coordinates and electronic energies of structures used in this paper, labeled structures and molecular graphs, and topological properties at ring critical points of interest.

AUTHOR INFORMATION
Corresponding Author
*E-mail: ignacy.cukrowski@up.ac.za

Notes

The authors declare no competing financial interest.

ACKNOWLEDGMENT

This work is based on the research supported in part by the National Research Foundation of South Africa (Grant Numbers 87777) and the University of Pretoria.

ABBREVIATIONS

QTAIM, Quantum Theory of Atoms in Molecules; NCI, Non-Covalent Interactions; IQA, Interacting Quantum Atoms; IQF, Interacting Quantum Fragments; AIL, Atomic Interaction Line; BP, Bond Path; NTA, Nitrilotriacetic acid; NTPA, Nitrilotri-3-propionic acid; BeNTA, $Be^{II}(NTA)^{-}$; BeNTPA, $Be^{II}(NTPA)^{-}$; BCP, Bond Critical Point; RCP, Ring Critical Point; CRn, Competition Reaction; LEC, Lowest Energy Conformer; SPFC, Single Point Frequency Calculation.

KEYWORDS

Complexes; Competition Reaction; Interacting Quantum Fragments; Preorganization; Binding.

REFERENCES

[1] A. E. Martell; R. D. Hancock, *Metal Complexes in Aqueous Solutions,* Plenum Press: New York, 1996.

[2] NIST Standard Reference Database 46. NIST Critically Selected Stability Constants of Metal Complexes Database, version 8.0; Database collected and selected by Smith, R. M., A.E.; US Department of Commerce, National Institute of Standards and Technology: Gaithersburg, MD, 2004.

[3] K. K. Govender; I. Cukrowski, *Inorg. Chem*. **2010**, *49*, 6931.

[4] I. Cukrowski; K. K. Govender; M. Mitoraj; M. Srebro *J. Phys. Chem. A* **2011**, *115,* 12746.

[5] C. O. da Silva; M. A. C. Nascimento *J. Phys. Chem. A* **1999,** *103*, 11194.

[6] G. A. A. Sarcino; R. Improta; V. Barone *Chemical Physics Letters* **2003**, *373,* 411.

[7] M. D. Liptak; K. C. Gross; P. G. Seybold; S. Feldgus; G. C. Shields *J. Am. Chem. Soc.* **2002**, *124*, 6421.

[8] M. Namazian; M. Zakery; M. R. Noorbala; M. L. Coote *Chemical Physics Letters* **2008**, *451*, 163.

[9] M. A. K. Liton; M. I. Ali; M. T. Hossain *Computational and Theoretical Chemistry*, **2012**, *999*, 1.

[10] C. P. Kelly; C. J. Cramer; D. G. Truhlar *J. Phys. Chem. A* **2006,** *110,* 2493.

[11] W. L. Jorgensen; J. M. Briggs *J. Am. Chem. Soc.* **1989,** *111*, 4190.

[12] K. K. Govender; I. Cukrowski *J. Phys. Chem. A* **2010**, *114*, 1868.

[13] K. K. Govender; I. Cukrowski *J. Phys. Chem. A* **2009,** *113,* 3639.

[14] M. Namazian; S. Halvani; M. R. Noorbala *Journal of Molecular Structure: THEOCHEM* **2004**, *711*, 13.

[15] W. Sanf-Aroon; V. Ruangpornvisuti *International Journal of Quantum Chemistry* **2008**, *108*, 1181.

[16] M. T. Benson; M. L. Moser; D. R. Peterman; A. Dinescu *Journal of Molecular Structure: THEOCHEM* **2008**, *867*, 71.

[17] M. D. Liptak,; G. C. Shields *International Journal of Quantum Chemistry* **2001**, *85*, 727.

[18] A. P. Harding; D. C. Wedge; P. L. A. Popelier *J. Chem. Inf. Model.* **2009,** *49,* 1914.

[19] M. S. Bodnarchuck; D. M. Heyes; D. Dini; S. Chahine; S. Edwards *J. Chem. Theory Comput.* **2014**, *10*, 2537.

[20] J. R. Pliego; J. M. Riveros *J. Phys. Chem. A* **2002,** *106,* 7434.

[21] R. D. Hancock; L. J. Bartolotti *Inorganica Chimica Acta* **2013**, *396*, 101.

[22] R. D. Hancock; L. J. Bartolotti *Inorg. Chem.* **2005**, *44*, 7175.

[23] R. D. Hancock ***Acc. Chem. Res.*** **1990**, *23*, 253.

[24] A. C. Alder; H. Siegrist; W. Gujer; W. Giger, *Wat. Res.***1990**, *24*, 733.

[25] J. F. Hainfield; W. Liu; C. M. R. Halsey; P. Freimuth; R. D. Powell *Journal of Structural Biology* **1999**, *127,* 185.

[26] R. D. Shannon *Acta Crystallogr Sect. A* **1976**, *A32*, 751.

[27] R. D. Hancock; A. S. de Sousa; G. B. Walton; J. H. Reibenspies *Inorg. Chem.* **2007**, *46*, 4749.

[28] V. J. Thom; C. C. Fox; J. C. A. Boeyens; R. D. Hancock *J. Am. Chem. Soc.* **1984**, *106*, 5947.

[29] T. W. Hambley *J. Chem. Soc., Dalton Trans.* **1986**, 565.

[30] R. D. Hancock; I. V. Nikolayenko *J. Phys. Chem. A* **2012**, *116*, 8572.

[31] R. D. Hancock *Chem. Soc. Rev.* **2013**, *42*, 1500.

[32] R. W. F.Bader *Atoms in Molecules: A Quantum Theory*, Oxford University Press: Oxford, U.K., 1990.

[33] R. F. W. Bader *J. Phys. Chem. A* **2009**, *113*, 10391.

[34] J. Cioslowski; S. T. Mixon *Can. J. Chem.* **1992**, *70*, 443.

[35] J. Cioslowski; S. T. Mixon *J. Am. Chem. Soc.***1992**, *114*, 4382.

[36] H. A.Jimenez-Vazquez; J. Tamariz; R. J.Cross *J. Phys. Chem. A* **2001**, *105*, 1315.

[37] K. Kobayashi; S. Nagase *Chem. Phys. Lett*. **2002**, *362*, 373.

[38] A. Haaland; D. J. Shorokhov; N. V. Tverdova *Chem.–Eur. J.* **2004**, *10*, 4416.

[39] M. J. Jablonski *J. Phys. Chem. A.* **2012**, *116*, 3753.

[40] E. Cerpa; A. Krapp; R. Flores-Moreno; K. J. Donald; G. Merino *Chem.–Eur. J.* **2009**, *15*, 1985.

[41] A. A. Popov; L. Dunsch *Chem.–Eur. J.* **2009**, *15*, 9707.

[42] P. Dem'yanov; P. Polestshuk *Chem.–Eur. J.* **2012**, *18*, 4982.

[43] J. Poater; M. Solà; F. M. Bickelhaupt *Chem.–Eur. J.* **2006**, *12*, 2889.

[44] J. Poater; M. Solà; F. M. Bickelhaupt *Chem.–Eur. J.* **2006**, *12*, 2902.

[45] J. Poater; R. Visser; M. Solà; F. M. Bickelhaupt *J. Org. Chem.* **2007**, *72*, 1134.

[46] A. Krapp; G. Frenking *Chem. Eur. J.* **2007**,*13*, 8256.

[47] S. Grimme; C. Mück-Lichtenfeld; G. Erker; G. Kehr; H. Wang; H. Beckers; H. Willner *Angew. Chem. Int. Ed.* **2009**, *48*, 2592.

[48] R. W. F. Bader *J. Phys. Chem. A* **2011**, *115*, 12432.

[49] C. F.Matta; J. Hernández-Trujillo; T. H. Tang; R. F. W. Bader; *Chem.–Eur. J.* **2003**, *9*, 1940.

[50] R. F. W. Bader *Chem.–Eur. J.* **2006**, *12*, 2896.

[51] R. F. W. Bader; D. C. Fang *J. Chem. Theory Comput.* **2005**, *1*, 403.

[52] M. von Hopffgarten; G. Frenking *Chem.–Eur. J.* **2008**, *14*, 10227.

[53] S. J. Grabowski; J. M. Ugalde *J. Phys. Chem. A.* **2010**, *114*, 7223.

[54] G. Frenking; M. Hermann; *Angew. Chem.* **2013**, *125*, 6036.

[55] D. Danovich; S. Shaik; H. S. Rzepa *Angew. Chem. Int. Ed.* **2013**, *52*, 5926.

[56] F. Weinhold *J. Comp. Chem.* **2012**, *33*, 2440.

[57] I. Cukrowski; J. H. de Lange; M. Mitoraj *J. Phys. Chem. A* **2014**, *118*, 623.

[58] I. Cukrowski; C. Matta *Chemical Physics Letters* **2010**, *499*, 66.

[59] P. R. Varadwaj; I. Cukrowski; C. B. Perry; H. M. Marques *J. Phys. Chem. A* **2011**, *115*, 6629.

[60] P. R.Varadwaj; I. Cukrowski; H. M. Marques *J. Phys. Chem. A* **2008,** *112*, 10657.

[61] P. R.Varadwaj; I. Cukrowski; H. M. Marques *Journal of Molecular Structure: THEOCHEM* **2009**, *902*, 21.

[62] E. R. Johnson; S. Keinan; P. Mori-Sánchez; J. Contreras-García; A. J. Cohen; W. Yang, *J. Am. Chem. Soc.* **2010**, *132*, 6498.

[63] J. Contreras-García; E. R. Johnson; S. Keinan; R. Chaudret; J. P. Piquemal; D. Beratan; W. Yang *J. Chem. Theory Comput.* **2011**, *7*, 625.

[64] N. Gillet; R. Chaudret; J. Contreras-García; W. Yang; B. Silvi; J. P. Piquemal *J. Chem. Theory Comput.* **2012**, *8*, 3993.

[65] J. Contreras-García; W. Yang; E. R. Johnson *J. Phys. Chem. A* **2011**, *115*, 12983.

[66] M. A. Blanco; A. M. Pendás; E. Francisco *J. Chem. Theory Comput.* **2005**, *1*, 1096.

[67] E. Francisco; A. M. Pendás; M. A. Blanco *J. Chem. Theory Comput.* **2006**, *2*, 90.

[68] A. M. Pendás; M. A. Blanco; E. Francisco *J. Comput. Chem.* **2006**, *28*, 161.

[69] (2010) *Spartan 10, Wavefunction Inc.*.Irvine, CA 92612, USA.

[70] M. J. Frisch, G. W. Trucks, H. B. Schlegel, G. E. Scuseria, M. A. Robb, J. R. Cheeseman, G. Scalmani, V. Barone, B. Mennucci, G. A. Petersson, H. Nakatsuji, M. Caricato, X. Li, H. P. Hratchian, A. F. Izmaylov, J. Bloino, G. Zheng, J. L. Sonnenberg, M. Hada, M. Ehara, K. Toyota, R. Fukuda, J. Hasegawa, M. Ishida, T. Nakajima, Y. Honda, O. Kitao, H. Nakai, T. Vreven, J. A. Montgomery, Jr., J. E. Peralta, F. Ogliaro, M. Bearpark, J. J. Heyd, E. Brothers, K. N. Kudin, V. N. Staroverov, R. Kobayashi, J. Normand, K. Raghavachari, A. Rendell, J. C. Burant, S. S. Iyengar, J. Tomasi, M. Cossi, N. Rega, J. M. Millam, M. Klene, J. E. Knox, J. B. Cross, V. Bakken, C. Adamo, J. Jaramillo, R. Gomperts, R. E. Stratmann, O. Yazyev, A. J. Austin, R. Cammi, C. Pomelli, J. W. Ochterski, R. L. Martin, K. Morokuma, V. G. Zakrzewski, G. A. Voth, P. Salvador, J. J. Dannenberg, S. Dapprich, A. D. Daniels, Ö. Farkas, J. B. Foresman, J. V. Ortiz, J. Cioslowski, and D. J. Fox, Gaussian 09, Revision D.1, Gaussian, Inc., Wallingford CT, 2009.

[71] . A. Keith, AIMAll (Version 13.11.04), TK Gristmill Software, Overland Parks KS, USA, 2013 (aim.tkgristmill.com).

[72] V. Tognetti; L. Joubert *J. Chem. Phys.* **2013**, *138*, 024102.

[73] X. Xu; W. A. Goddard, *Proc. Natl. Acad. Sci.* USA, **2004**, *101*, 2673.

[74] J. P. Perdew; K. Burke; M. Ernzerhof *Phys. Rev. Lett.* **1996**, *77*, 3865.

[75] I. Hyla-Kryspin; G. Haufe; S. Grimme *Chem. Eur. J.* **2004**, *10*, 3411.

[76] B. Hammer; L. B. Hansen; J. K. Nørskov *Phys. Rev. B* **1999**, *59*, 7413.

[77] Y. Zhang; W. Yang *Phys. Rev. Lett.* **1998**, *80*, 890.

[78] S. N. Maximoff; J. E. Peralta; V. Barone; G. E. Scuseria, *J. Chem. Theory Comput.* **2005,** *1*, 541.

[79] W. Humphrey; A. Dalke; K. *J.* Schulten *Molec. Graphics* **1996**, *14*, 33.

[80] I. Cukrowski; J. H. de Lange; A. S. Adeyinka; P. Mangondo *Comput. Theoret. Chem.* **2015**, *1053*, 60.

[81] Varadwaj, P. R.; Varadwaj, A.; Peslherbe, G. H.; Marques H. M. *J. Phys. Chem. A.* **2011**, *115*, 13180–13190.

[82] M. P. Mitoraj; A. Michalak; T. Ziegler *J. Chem. Theory Comput.* **2009**, *5*, 962.

[83] M. P. Mitoraj; A. Michalak; T. Ziegler *Organometallics* **2009**, *28*, 3727.

[84] M. P. Mitoraj *J. Phys. Chem. A* **2011**, *115*, 14708.

[85]R. F. W. Bader; C. F. Matta *J. Phys. Chem A.***2006,** *110, 6365.*

[86] R. McWeeny *Methods of Molecular Quantum Mechanics*, 2nd ed., Academic Press, London, 1992.

[87] A. M. Pendás; M. A. Blanco; E. Francisco *J. Chem. Phys.* **2006**, *125*, 184112.

[88] G. Frenking; K. Wichmann; N. Fröhlich; J. Grobe; W. Golla; D. Le Van; B. Krebs; M. Läge *Organometallics* **2002**, *21*, 2921.

[89] R. A. Fischer; M. M. Schulte; J. Weiss; L. Zsolnai; A. Jacobi; G. Huttner; G. Frenking; C. Boehme; S. F. Vyboishchikov *J. Am. Chem. Soc.* **1998**, *120*, 1237.

Table of Contents Synopsis and Graphic

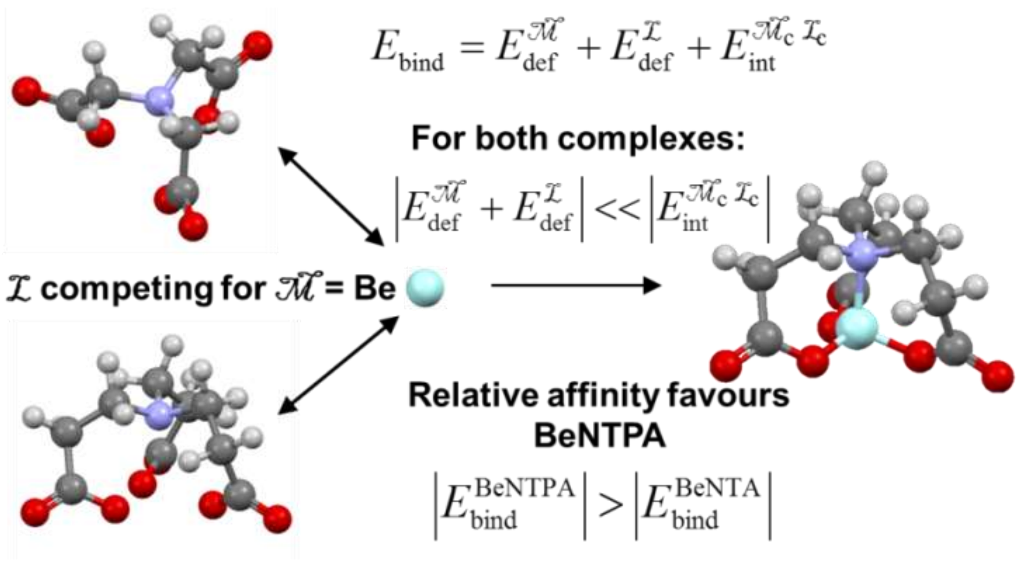

This methodology accounts for the total energy contributions coming from all atoms of selected molecular fragments. By decomposing changes in *e.g.*, fragment deformation, inter- and intra-fragment interaction energies, the origin of complexes relative stability was identified. Although coordination bonds' strength favours BeNTA, the origin of BeNTPA being more stable was found to be due to less sever repulsive interactions with the backbone of NTPA (C and H-atoms).

Supplementary Information

Part 1:

Procedure for determining theoretical equilibrium constants for the competition reaction

It is important to stress that our aim here is not to find an accurate prediction of formation constants, but rather to select a level of theory which confirms the experimental trend (the preferential formation of BeNTPA) and thus validates the theoretically/computationally generated structures. To this effect, the competition reaction-based protocol proposed previously[1] to computationally predict the formation constants, was adopted in this work. For clarity, only the most important steps are presented here.

The complex formation reactions between beryllium and the ligands of interest are shown as reactions (S1) and (S2) with relevant equilibrium constants, K_1^{NTPA} and K_1^{NTA} (charges have been omitted throughout for simplicity)

$$\mathrm{Be(H_2O)_4 + NTPA \leftrightarrow BeNTPA + 4H_2O} \qquad K_1^{\mathrm{NTPA}} = \frac{[\mathrm{BeNTPA}]}{[\mathrm{Be}][\mathrm{NTPA}]} \tag{S1}$$

$$\mathrm{Be(H_2O)_4 + NTA \leftrightarrow BeNTA + 4H_2O} \qquad K_1^{\mathrm{NTA}} = \frac{[\mathrm{BeNTA}]}{[\mathrm{Be}][\mathrm{NTA}]} \tag{S2}$$

A competition reaction, CRn, between ligands NTPA and NTA for $\mathrm{Be^{II}}$, can be viewed as a result of subtraction of the two complexation reactions, (S1) – (S2), where the participation of water is conveniently cancelled; this is shown as reaction (S3) with expression for the CRn equilibrium constant, K_1^{CRn}

$$\mathrm{BeNTA + NTPA \leftrightarrow BeNTPA + NTA} \qquad K_1^{\mathrm{CRn}} = \frac{[\mathrm{BeNTPA}][\mathrm{NTA}]}{[\mathrm{BeNTA}][\mathrm{NTPA}]}. \tag{S3}$$

Because the formation constants of both complexes are known from experiment ($\log K_1^{\mathrm{NTPA}}$ = 9.23 and $\log K_1^{\mathrm{NTA}}$ = 6.84),[2] one can determine the equilibrium constant, as $\log K_1^{\mathrm{CRn}}$, for the competition reaction from

$$\log K_1^{\mathrm{CRn}} = \log \frac{K_1^{\mathrm{NTPA}}}{K_1^{\mathrm{NTA}}} = \log K_1^{\mathrm{NTPA}} - \log K_1^{\mathrm{NTA}} = 2.4. \tag{S4}$$

Hence, using the well-known relationship, $\Delta G = -\mathrm{R}T\ln K$, which correlates thermodynamic Gibbs free energy and equilibrium constant, and by converting one log unit to 1.36 kcal/mol, it is possible to determine the ΔG value expected from experiment for any reaction and, in our case, one obtains ΔG_{CRn} = –3.3 kcal/mol. This information is useful because one can attempt to reproduce this value theoretically by computing the free energy of the competition reaction (S3) as

$$\Delta G_{\mathrm{CRn}} = G(\mathrm{BeNTPA}) + G(\mathrm{NTA}) - G(\mathrm{BeNTA}) - G(\mathrm{NTPA}) \tag{S5}$$

It has been shown that the best theoretically predicted values of stepwise protonation constants,[3],[4] as $\log K_{\mathrm{H}}^{(\mathrm{n})}$, (where n = 1,2,… represents the number of the consecutive stepwise protonation reaction) and the complex formation constants,[1] as $\log K_1$, are obtained when the lowest energy conformers (LECs) of the molecules are selected for the calculation. Thus all conformers of the ligands and the complexes found from conformational search in SPARTAN have been optimized at the MP2 level of theory in water as a solvent.

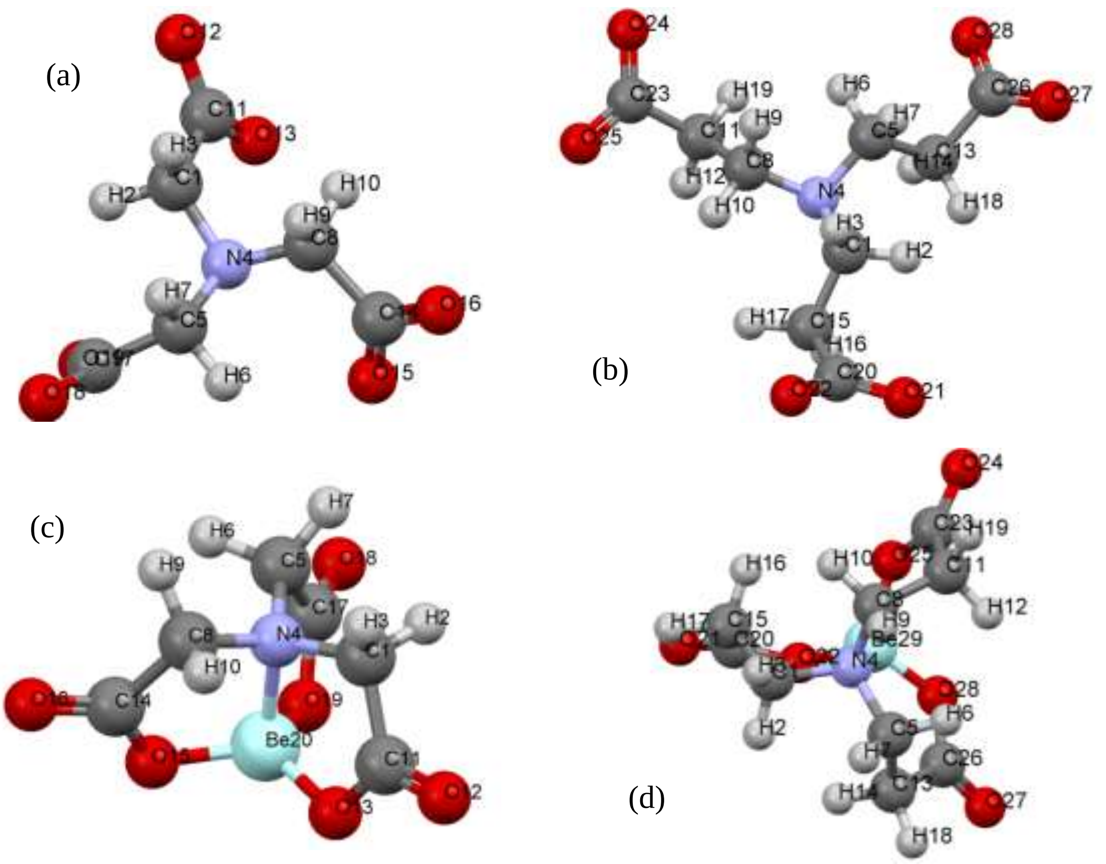

Figure S4. The lowest energy conformers of the free ligands: NTA – part (a), NTPA – part (b). and $\mathrm{Be^{II}}$ complexes: BeNTA – part (c) and BeNTPA – part (d).

Consequently, only the LECs of complexes and ligands shown in Figure S1 were selected for further theoretical investigations. The G values for all components of the CRn (S3) together with the computed $\log K_1^{\text{CRn}}$ value are shown in Table S1.

Table S1. Computed equilibrium constant, as $\log K_1^{\text{CRn}}$, for competition reaction between ligands NTPA and NTA for Be^{II}; lowest energy conformers of the ligands and complexes were used.

Method	G/au				ΔG_{CRn} [a]	$\log K_1^{\text{CRn}}$	$\Delta \log K$ [b]
	BeNTA	NTPA	BeNTPA	NTA			
MP2	–751.7060	–854.5841	–869.2266	–737.0736	–6.4	4.7	2.3

[a] Value in kcal/mol. [b] $\Delta\log K$ = (theoretical – experimental) value.

The data shown in Table S1 validates the structures of ligands and complexes, correlating well with the experimental trend. However, one must remember that a number of computational techniques, such as for the quantum chemical topology techniques QTAIM and IQA, can only partition the electronic energy (but not the Gibbs free energy) into atomic and interatomic contributions. Hence, to select the most suitable level of theory, it was necessary to compute the change in the electronic energy, ΔE_{CRn} – see expression (S6).

$$\Delta E_{\text{CRn}} = E(\text{BeNTPA}) + E(\text{NTA}) - E(\text{BeNTA}) - E(\text{NTPA}) \qquad \text{(S6)}$$

Furthermore, in order to have the structural benefit of the MP2-generated conformers and avoid computationally expensive IQA calculations at this level of theory, we performed SPCs in solvent on the MP2-optimized structures at selected DFT levels of theory to compute electronic energies and to generate the wavefunctions necessary for the QTAIM/IQA calculations. Importantly, as data included in Table S2 shows, the preferential formation of BeNTPA is reproduced correctly at all levels of theory when the change in electronic energy is considered. Hence, in principle, it was possible to explore the topological properties (QTAIM, NCI and IQA) of the structures of interest at any level of theory.

Table S2. Computed ΔE_{CRn}, for the competition reaction for beryllium ion using the lowest energy conformers of the ligands and complexes of NTA and NTPA.

Method	E(aq)/au				ΔE_{CRn} [c]
	Be(NTA)	NTPA	Be(NTPA)	NTA	
MP2[a]	–751.8053	–854.7518	–869.4101	–737.1610	–8.8
PBE1PBE[b]	–752.8958	–856.0522	–870.7279	–738.2275	–4.7
B3LYP[b]	–753.7321	–857.0189	–871.7112	–739.0440	–2.7
X3LYP[b]	–753.4405	–856.6684	–871.3552	–738.7590	–3.4

[a]Energies of the lowest energy conformer of each molecule. [b]Electronic energies obtained by performing a single point calculation on the RMP2 optimized structures. [c]Values in kcal/mol.

REFERENCES

[1] K. K. Govender; I. Cukrowski, *Inorg. Chem*. **2010**, *49*, 6931.

[2] NIST Standard Reference Database 46. NIST Critically Selected Stability Constants of Metal Complexes Database, version 8.0; Database collected and selected by Smith, R. M., A.E.; US Department of Commerce, National Institute of Standards and Technology: Gaithersburg, MD, 2004.

[3] K. K. Govender; I. Cukrowski *J. Phys. Chem. A* **2010**, *114*, 1868.

[4] K. K. Govender; I. Cukrowski *J. Phys. Chem. A* **2009,** *113*, 3639.

Part 2:

Preliminary Investigations

Geometric Analysis

We will start our investigation with a brief analysis of geometric factors which are commonly used to rationalize relative trends in formation constants. The good approximation of the $\log K_{\mathrm{CRn}}$ and ΔE_{CRn} gave us the confidence to use the MP2 optimized structure for this purpose. We performed a full geometric evaluation of the complexes based on the length of the coordination bonds, presence/absence of steric contacts and comparison of computed structures with the minimum strain geometry criteria.[1]

Coordination Bonds. Classically it has been suggested that the complex with the shorter (hence most likely stronger) coordination bonds has also stronger overall binding energy between the ligand and a metal ion. Note that NTA and NTPA have the same kind and number of donor atoms as well as binding of metal to a ligand takes place in very much the same molecular environment; hence, such a presumption should hold in this case. Data presented in Table S3 shows that in both complexes d(Be,O) << d(Be,N); this suggests that the coordination bonds with O-atoms are significantly stronger and results are inconclusive because |Δd(Be,O)| = 0.002 Å is only marginally in favour of BeNTPA whereas |Δd(Be,N)| = 0.02 Å is decisively in favour of BeNTA.

Table S3. Selected average interatomic distances in both complexes at the MP2 level of theory.

BeNTA		BeNTPA	
Bond	d / Å	Bond	d / Å
Be–N	1.772	Be–N	1.791
Be–O13	1.612	Be–O22	1.610
Be–O15	1.612	Be–O25	1.610
Be–O19	1.612	Be–O28	1.610

Repulsive Contacts. Surprisingly, there are three severe CH--HC contacts present in the stronger BeNTPA complex (d(H,H) = 2.159±0.001 Å) whereas there are three weak contacts in BeNTA, d(H,H) = 2.331±0.002 Å (see data in Table A7 in Appendix A). The absence of steric close contacts, such as CH--HC, is quite often identified as the cause for preferential complex formation.[1–4] If there are short contacts between hydrogen atoms, with interatomic distance much shorter than the sum of the van der Waals radii, 2.4 Å, there is said to be an interaction which destabilizes the molecule, commonly referred to as steric hindrance. The computed difference |Δd(H,H)| = 0.172 Å between interatomic distances observed in both complexes, however, favours BeNTA which clearly contradicts experimental data in terms of a trend in relative stability. Thus, we do not have *structural* evidence to suggest that the CH--HC contacts in BeNTPA result in the steric hindrance phenomenon because this complex is more stable. Additionally, it is difficult to determine the energetic effect of the CH--HC contacts on the formation of BeNTPA because they are present in LEC NTPA where d(H,H) = 2.108±0.001 Å.

Table S4. Selected interatomic distances for steric contacts in both complexes at the RMP2 level of theory.

BeNTA		BeNTPA	
Interaction	d / Å	Interaction	d / Å
N•••O13	2.568	N•••O22	2.753
N•••O15	2.568	N•••O25	2.753
N•••O19	2.566	N•••O28	2.753
O13•••O15	2.760	O25•••O28	2.653
O15•••O19	2.762	O25•••O22	2.653
O13•••O19	2.761	O22•••O28	2.653
H2•••H7	2.332	H2•••H14	2.160
H6•••H9	2.329	H6•••H12	2.159
H3•••H10	2.332	H10•••H16	2.157

Relative complex stability has also been associated with the repulsion between lone pairs on donor atoms.[1] However, as far as we are aware, there has been no extensive investigation into the effect of the lone pair donor atoms. We assumed that the shorter the interatomic distance, the greater the repulsion and when the interatomic distance is shorter than the sum of van der Waals radii (d_{vdw}(N,O) = 3.1 Å and d_{vdw}(O,O) = 3.0 Å) then it is reasonable to consider this as a repulsive interaction. Table S4 shows that in both complexes the N--O and O--O contacts are much shorter than the respective sum of the van der Waals radii. Furthermore, the N--O contacts of 2.567 Å in BeNTA are much shorter, by ~0.19 Å, than those in BeNTPA which suggests that they result in greater repulsion in BeNTA. The O--O contacts of 2.653 Å, on the other hand, are shorter in BeNTPA than in BeNTA by ~0.11 Å which suggests that in this case the repulsion is more severe in BeNTPA. Because the results produced are mixed, depending on the type of a contact, it is not possible to predict geometrically which complex is preferentially formed in a solution.

Minimum Strain Geometries. Minimum strain geometries, obtained using experimental data and molecular mechanics calculations, have been used to describe the preferential complex formation and explain the favourable complexing of small metal cations when 6m-CRs are formed while larger metal cations favourably complex to form 5m-CRs.[1] Any deviation from these minimum strain geometries would be indicative of an increase in strain, hence the greater the deviation, the greater the strain. The results of these comparisons (Table S5) reveal that BeNTA consistently shows the greater deviation which is consistent with the experimental trend in log$K$ values. However, when the same approach was used to compare strain induced by departure from ideal geometries in Nickel[5] and Zinc[6] complexes, it was found that the N–M–O bite angles in the NTA complexes consistently had a greater deviation from the ideal values, whereas those in NTPA were comparable to the minimum strain geometries; a trend which is exactly the same as observed for Be^{II} complexes with NTA and NTPA. This indicates that while there has been success in the instances of the beryllium complexes, this approach is not universal and may even be misleading.

Table S5. Selected structural properties of the complexes for the comparison with minimum strain geometries (shown in brackets).

	BeNTA		BeNTPA	
Bond	d / Å	Δd	d / Å	Δd
Be–N	1.772 (2.5)	–0.728	1.791 (1.6)	0.191
Be–O	1.612 (>3.2)	–1.588	1.610 (1.9)	–0.290
Bond Angle	Angle / deg	Δ(angle)	Angle / deg	Δ(angle)
Be–N–C	102.24 (109.5)	–7.26	109.82 (109.5)	0.32
Be–O–C	112.21 (126)	–13.79	122.64 (126)	–3.36
O–Be–N (N–M–N)	102.24 (69)	33.24	107.96 (109.5)	–1.54
O–Be – N (O–M–O)	102.24 (58)	44.24	107.96 (95)	12.96

Overall, it is clear that the three geometric approaches, namely (i) strength of bonding based on coordination bond length, (ii) destabilization due to steric contacts, such as CH--HC in the framework of a ligand and N--O or O--O in the coordination sphere, and (iii) deviation from the minimum strain geometry, do not provide rigorous and reliable account for the preferential complex formation. Hence, there is a need to use alternative and more advanced (computationally based) methods to fundamentally investigate relative stability of complexes and molecular systems in general.

QTAIM Analysis of Intramolecular Interactions

The molecular graphs of both LECs complexes are shown in Figure S2 where AILs (they represent a line of maximum electron density joining two atoms) are observed only between atoms bonded through covalent and coordination bonds; hence, these interactions can be seen in this case as real bond paths which fully correlate with chemists' understanding of chemical bonding. Because the topological properties at the bond critical points (BCPs) of the bond paths were successfully used to characterize and classify many chemical bonds, we will compare the nature and strength of bonding in the coordination sphere of both complexes with an attempt to rationalize the preferential complex formation. Furthermore, we will attempt to evaluate properties of 5- and 6-membered chelate rings using topological properties at the ring critical points (RCPs).

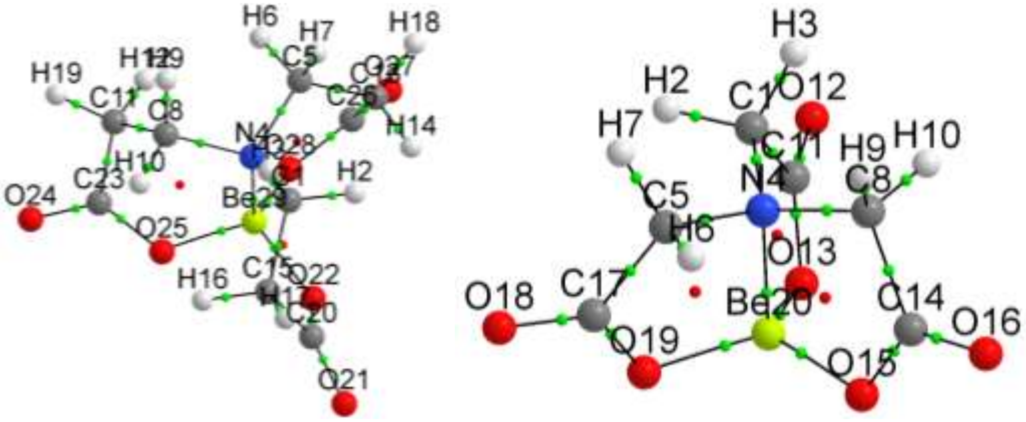

Figure S2. The QTAIM molecular graphs of (a) the lowest energy conformer of BeNTPA, and (b) the complex of BeNTA.

Coordination bonds. Table S6 shows the topological properties of the coordination bonds at the BCPs. The values of $\rho(\boldsymbol{r})$ and Laplacian, $\nabla^2\rho(\boldsymbol{r})$, at the BCPs in both complexes, are consistent with those expected to be for closed-shell, non-covalent interactions.[7] The ratio of the local potential energy density $V(\boldsymbol{r})$ to the local kinetic energy density $G(\boldsymbol{r})$ has also been frequently and successfully used[8-10] as a descriptor of the nature of the bonding between two atoms. When $|V(\boldsymbol{r})|/G(\boldsymbol{r}) < 1$, this is typical of a classical ionic (or closed shell) interaction and when $|V(\boldsymbol{r})|/G(\boldsymbol{r}) > 2$, it is indicative of a classical covalent bond.

Based on the characteristics of the electron density at the BCPs, all coordination bonds show borderline behaviour of classical ionic character with the $|V(\boldsymbol{r})|/G(\boldsymbol{r})$ ratio very close to 1; the Be–N bonds show some degree of covalency. The electron density at BCP has been used[5,6,11] to measure the bond strength between two atoms. For both complexes, ρ_{BCP}(Be–O) > ρ_{BCP}(Be–N) and this is consistent with results found for the Zn complexes.[4] However, by comparing the ρ_{BCP} values of the coordination bonds in BeNTA and BeNTPA, it is clear that the electron density is somewhat greater in all coordination bonds of BeNTA which suggests that the binding of NTA to beryllium is stronger; this is in accord with a chemist's intuition because the more chemical glue, *i.e.* electron density between atoms, the stronger bond is expected to be.

Table S6. QTAIM-defined topological data at BCPs of the coordination bonds in BeNTA and BeNTPA at the RMP2[a] level of theory.

Bonds	$\rho(r)$	$\nabla^2\rho(r)$	$G(r)$	$V(r)$	$\|V(r)\|/G(r)$	DI(A|B)
			BeNTA			
Be–N	0.0636	0.3775	0.1019	–0.1095	1.07	0.11
Be–O13	0.0771	0.5655	0.1418	–0.1423	1.00	0.14
Be–O15	0.0771	0.5656	0.1419	–0.1423	1.00	0.14
Be–O19	0.0771	0.5655	0.1418	–0.1423	1.00	0.14
			BeNTPA			
Be–N	0.0598	0.3453	0.0917	–0.0971	1.06	0.11
Be–O22	0.0755	0.5660	0.1402	–0.1389	0.99	0.14
Be–O25	0.0755	0.5659	0.1402	–0.1388	0.99	0.14
Be–O28	0.0755	0.5660	0.1402	–0.1389	0.99	0.14

[a] all values are in au except $|V(r)|/G(r)$ and DI(A|B).

It is now well established that an exponential decrease should be observed for ρ_{BCP} plotted against an interatomic distance when an interaction of interest takes place in similar (comparable) molecular environment. In an attempt to reconcile the geometric (shorter bond length) and the QTAIM (larger ρ_{BCP}) notions of coordination bond strength we correlated the ρ_{BCP} with the corresponding interatomic distances (note that, due to molecular symmetry of ligands, there are not sufficient data points to generate a meaningful graph). Considering Be–N coordination bonds, as expected, the shorter bonds have larger ρ_{BCP}. However, this trend does not hold for Be–O coordination bonds. This clearly indicates that some other physical properties, most likely related to differences in highly crowded environment of the coordination spheres, must have contributed to the reverse trend in density at these critical points. Following the classical notion of chemical bonding and using accumulated density in the bonding region, ρ_{BCP}, as a measure of the strength of the coordination bonds one might reason that BeNTA should be the preferentially formed complex, again a misleading prediction. This leads us to the conclusion that one cannot use a coordination bond length or

ρ_{BCP} of the coordination bonds as a rigorous, universal and reliable tool in predicting relative complex strength as measured by log*K* values.

Ring Critical Points. In previous works[5,6] a good correlation was found between the electron density at the RCPs of the chelating 5- and 6-membered ring and the formation constant, as log*K* value, of the NTA and NTPA complexes with Ni^{II} and Zn^{II}. Table S7 shows the electron densities as well as the value of the Laplacian at the ring critical points found for the Be^{II} complexes with NTA and NTPA. This data reveals that the trends in ρ_{RCP} are the same in these complexes, namely ρ_{RCP}(MNTPA) < ρ_{RCP}(MNTA) and the ratio ρ_{RCP}(MNTA): ρ_{RCP}(MNTPA) is approximately two, regardless of the identity of the metal ion (here M = Be^{II}, Ni^{II}, Zn^{II}) and regardless of which complex (here ligand = L = NTA, NTPA) is formed preferentially (similar observations fully apply to the Laplacian at RCPs). It would be of great interest and fundamental importance in the ligand design strategies to find out whether such relationship is of general nature, *i.e.* does it also hold for (i) other metal ions for which formation constants with NTA and NTPA are known, and (ii) for other ligands which form 5m- and 6m-CRs.

Table S7. QTAIM-defined topological data at RCPs of chelating rings in BeNTA and BeNTPA at the RMP2[a] level of theory.

BeNTA			BeNTPA		
Atoms	$\rho(r)$	$\nabla^2\rho(r)$	Atoms	$\rho(r)$	$\nabla^2\rho(r)$
N4-C5-C17-O19-Be20	0.0336	0.1658	N4-C5-C13-C26-O28-Be29	0.0184	0.0886
C1-N4-Be20-O13-C11	0.0336	0.1654	N4-C8-C11-C23-O25-Be29	0.0184	0.0887
N4-C8-C14-O15-Be20	0.0336	0.1652	C1-N4-Be29-O22-C20-C15	0.0184	0.0887
av:	*0.0336*	*0.1655*	*av:*	*0.0184*	*0.0887*

[a] all values are in au.

Based on the additional findings of this work and noting that coordination rings differ only by the presence of an additional $–CH_2$- fragment we suggest that the topological properties at the ring critical point depend predominantly on the size of the ring under consideration. One might reason that the larger the ring, the more room there is for electron density to decrease from the bond paths' critical points to the ring critical point; hence, consistently one observes ρ_{RCP}(6m-CR) << ρ_{RCP}(5m-CR) but one does not know yet whether the ratio, ρ_{RCP}(5m-CR)/ ρ_{RCP}(6m-CR) depends on a central metal ion and to what extent. To conclude this section, it is clear that the value of ρ_{RCP} cannot be used to confidently predict the relative strength of metal complexes involving the NTA and NTPA ligands.

NCI Analysis

The inconclusive results of the above analyses strongly suggest that, besides geometric and topological parameters (the latter generated from the QTAIM analysis), there must be some other factors controlling or influencing the relative stability of molecular systems. It is important to note that although there are numerous, geometrically-detected, close interatomic contacts in both complexes, they are not characterised by the presence of AILs. This is not entirely surprising because BPs were shown to represent the privileged exchange-correlation channels;[12] hence, often one (i) does not observe a BP-linked atoms for which a geometrical criterion is met, as is the case in this work, or (ii) see a BP linking atoms being further apart even though other and shorter analogous contact(s) exist in the same molecular environment – an example of that is shown in Figure S3.

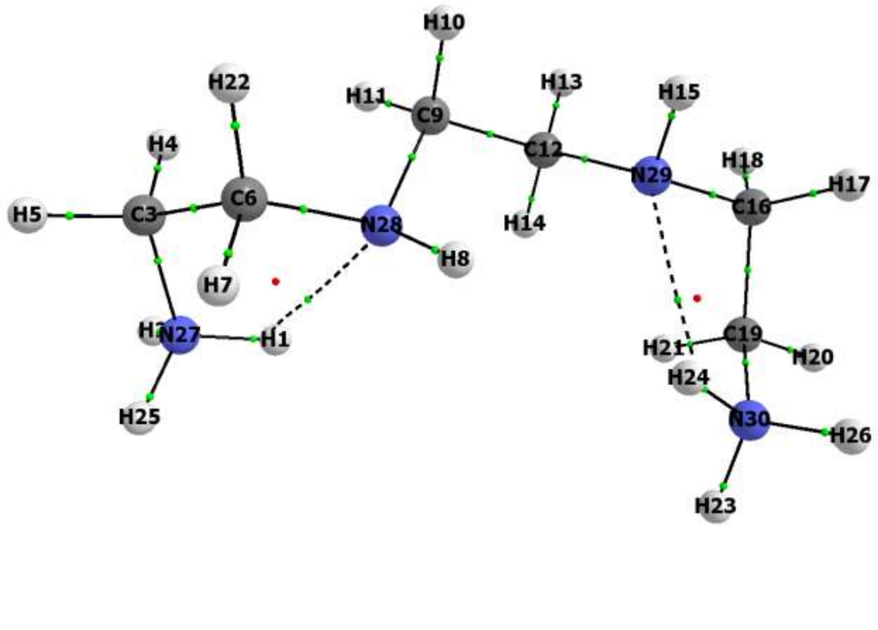

Figure S3. An example of an AIL linking atoms N29 and H24 with d(N,H) = 2.566 Å even though in the same environment atoms N29 and H8 with d(N,H) = 2.511 Å are present and they are not linked by AIL

To address shortcomings of the QTAIM-based analysis of intramolecular interactions, we turned our attention to the recently developed NCI method, which enables the real space visualization of non-covalent interactions in molecular systems[13–16]. An attractive feature of this technique lies in the ability to recover non-covalent weak interactions as defined in the QTAIM regime as well as other interactions not visualized in QTAIM and this produces the full picture of intramolecular interactions. This technique, using the reduced density gradient, s, and the sign of the second eigenvalue, λ_2, of the Hessian Matrix, has been used to distinguish between attractive and repulsive interactions. The colour-coded isosurfaces in Figure 3.3 indicate a local (i) accumulation of electron density as a blue region when $\lambda_2 < 0$ (then a negative trough in the NCIPlot is observed), a typical NCI index used to identify stabilizing interactions, and (ii) depletion of electron density as a red region when $\lambda_2 > 0$, a NCI index for destabilizing or non-bonded interactions (a positive trough in the NCIPlot is then observed) often interpreted as steric repulsion.[13–16,17]

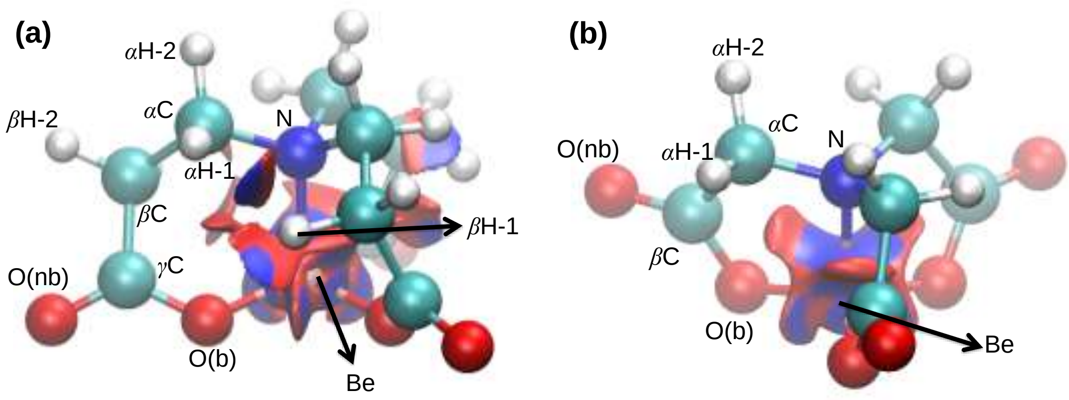

Figure S4. The NCI isosurfaces of the LECs of (a) BeNTPA, and (b) BeNTA complexes with a RDG isovalue of 0.5 au and isosurfaces coloured from blue to red using -0.07 au $\leq$ sign(λ_2)$\times\rho(r) \leq +0.03$ au.

Let us first focus on the coordination spheres of complexes. The NCI isosurfaces in Figure S4 show that all coordination bonds are characterized by large blue regions in the bonding region, indicative of electron density accumulation. Thus the NCI-based interpretation as stabilizing interaction fully recovers a general notion of coordination bonds. These blue regions appear to be immersed in sheet-like extended surfaces, the results of multi-centric interactions taking place in this crowded environment. This extended multi-surface NCI plot is coloured in red and this might be interpreted as revealing strain in the coordination sphere. Interestingly and importantly, a similar phenomenon of density accumulation is also observed between the lone pairs of the donor atoms in the coordination sphere. Notice that the O•••O interactions have blue surfaces in the interatomic region which, as also observed for the coordination bonds, are part of the extended red surface in the coordination sphere which supports our interpretation of the coordination sphere being strained. A similar phenomenon was found in the case of non-equilibrium water and ammonia dimer conformations, where a large blue disk was found between water dimers[18] and nitrogen atoms[17] in a repulsive arrangement. One must realize, however, that (i) any density accumulation might be a result of either a bonding interaction or unavoidable output of an "excess" of electron density, such as a free pair of electrons in a crowded environment, and (ii) a density accumulation must be accompanied by an adjacent region from which density was depleted. Hence, even though a red region of electron density depletion in crowded environments was interpreted as the presence of steric repulsion,[8,16] each case, in our opinion, must be analysed separately and interpreted with outmost care. What is unquestionable, however, is the physical meaning of the blue/red regions which simply uncovers locally increased/decreased density which directly points at non-covalently interacting atoms. Furthermore, one observes a blue area in the interatomic region between O(b) and βH1 in BeNTPA and this can be interpreted as the result of attractive interaction occurring just at the edge of coordination sphere, hence this constitutes a part of the extended polycentric isosurface.

Figure S4 also reveals that there are no interactions outside of the coordination sphere in the BeNTA complex. This finding is important because it implies that there are no additional (whether attractive or repulsive) interactions within a ligand framework, hence the short CH--HC contacts identified from the geometrical analysis do not play any role on complex stability (they neither de- nor stabilize BeNTA).

Conversely, the NCI-analysis uncovers the presence of many additional intramolecular interactions outside the coordination sphere of the BeNTPA complex which were 'missed' by the QTAIM-based interpretation. For all CH•••O and CH•••HC interactions (they are distributed uniformly around the molecule) we observe in Figure S4 classical in the NCI-interpretations bi-centric in nature and bi-coloured pill-like isosurfaces with blue region being placed in the interatomic region and red end pointing at a location of a potential ring critical point, where lowest density is observed within a ring. The work of Lane *et al.* [17] found numerous interactions (CH•••O, CH•••N, NH•••H, NH•••OC) which they described as ring closure, which are similar to our CH•••O and CH•••HC interactions. Their work[17] revealed the presence of classical OH•••O interactions in (a) 1,2-ethanediol, even though a bond path and associated BCP and RCP were absent, and (b) 1,3-propanediol and 1,4-butanediol, where AILs were present. The interactions were qualitatively indistinguishable and the only significant difference was in the minimum values of the reduced density gradient, $s_{\min}$. In principle, very much the same picture was found for the CH•••O and CH•••HC interactions in BeNTPA – see NCI plots in Figure S5(a) where the CH•••HC interaction is characterized by negative trough (corresponding to an attractive interaction and the blue isosurface) being placed at more negative value of sign(λ_2)×ρ and s_{min} closer to 0 when compared with the NCI plot obtained for the CH•••O interaction. The shape and placement of troughs in Figure S5(a) might indicate, besides larger density at NCI-defined critical point, that the density accumulation in the bonding region of the CH•••HC interaction is better defined in terms of a special shape.

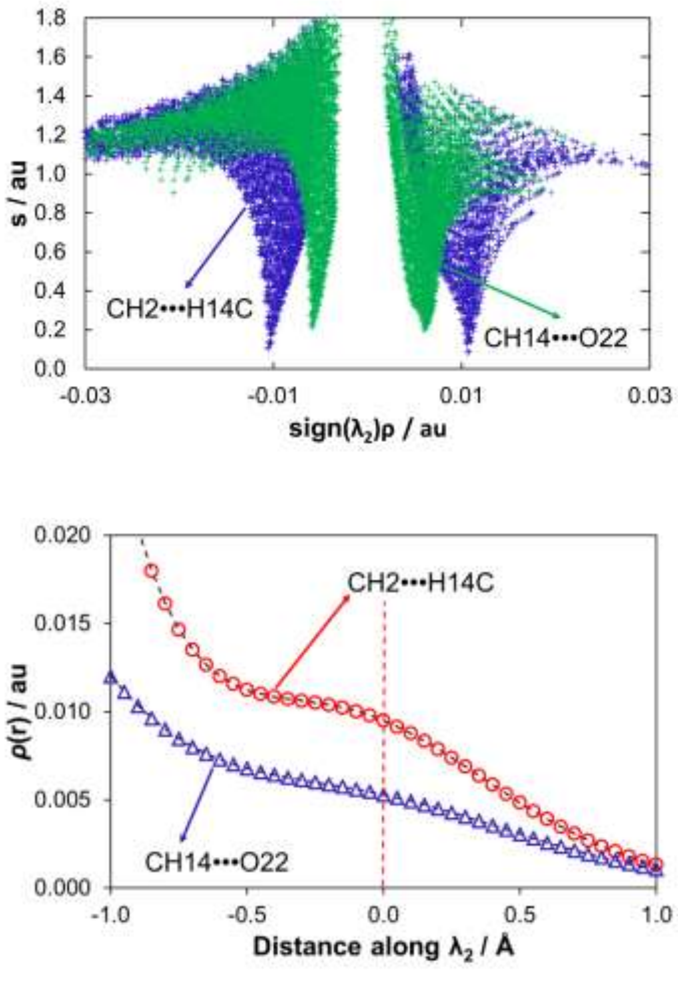

Figure S5. (a) The 2D NCI plots for selected CH•••HC and CH•••O interactions in the BeNTPA complex. (b) The corresponding cross-sections of the electron density along the λ_2 eigenvector where the red line indicates the GIP.

In search for qualitative differences between the CH•••O and CH•••HC intramolecular interactions in BeNTPA and to gain further insight on density distribution in their bonding regions we decided to employ recently reported 1D cross-section along the λ_2 eigenvector of the Hessian matrix.[18] This methodology was also shown to be able to explain the presence/absence of an AIL between atoms being at an interatomic distance shorter than the sum of the van der Waals radii. Results obtained from cross-sections, shown in Figure S5(b), lead to the following observations: (i) in both cases, locally concentrated density at any point of the cross-section is lower when compared with the preceding point which fully explains the absence of an AIL,[18] (ii) the density at the geometric critical point (placed in the middle between the interacting atoms) is indeed significantly larger in the case of the CH•••HC interaction as also found from the NCI plots, (iii) the shape of the cross-section obtained for the CH•••HC interaction (in Figure S5(b)) is by far better defined in terms of density accumulation represented by clearly visible hump, and finally (iv) qualitatively, there appears to be no difference in the density distribution in the bonding regions of these two interactions; a steady decrease in accumulated density is observed.

The following commonly accepted classical interpretations might be considered, namely (i) the intramolecular OH•••O interaction (a classical intramolecular H-bond) adds to the molecule's stability and (ii) the blue NCI-defined region of density accumulation is synonymous with stabilizing interaction. In view of these interpretations, in conjunction with the observation that there is no qualitative difference in the results obtained from the NCI and cross-section methodologies when applied to these two intramolecular interaction, one might tentatively conclude that since these features hold for the stabilizing CH•••O interaction, then there is no obvious reason to interpret the CH•••HC interaction differently, both in the BeNTPA complex. If this is so, then one might also postulate that maybe the preferential complexation of BeNTPA is due to the additional stabilization of the complex by CH•••O and CH•••HC. However, as also strongly advocated in a recent report[18] these suppositions must be supported by additional physical properties and we turn our attention to IQA for further insight.

IQA-based Analysis of Diatomic Interactions in the Complexes

The IQA method partitions the molecular energy, E, into one-body (atoms of a molecule) and two-body (interatomic) interaction energy components.[19–21] In the simplest way, E can be partitioned into additive atomic energy for each atom X, $E_{\mathrm{add}}^{\mathrm{X}}$, such that

$$E = \sum_{\mathrm{X}} E_{\mathrm{add}}^{\mathrm{X}} \tag{S7}$$

The additive atomic energy is defined as the sum of the self-energy of an atom and halved sum of interaction energies with remaining atoms in a molecule as described by Eq. S8

$$E_{\mathrm{add}}^{\mathrm{X}} = E_{\mathrm{self}}^{\mathrm{X}} + \sum_{\mathrm{Y}\neq\mathrm{X}} 0.5E_{\mathrm{int}}^{\mathrm{X,Y}} \qquad \text{(S8)}$$

Hence, as shown in Eq. S9, the energy of a molecule can be recovered by summing up all self-atomic energies and all unique diatomic interaction energies,

$$E = \sum_{\mathrm{X}} E_{\mathrm{self}}^{\mathrm{X}} + 0.5\sum_{\mathrm{X}}\sum_{\mathrm{Y}\neq\mathrm{X}} E_{\mathrm{int}}^{\mathrm{X,Y}} \qquad \text{(S9)}$$

One of the attractive features of IQA is the information one can gain about the strength of any diatomic interaction (from $E_{\mathrm{int}}^{\mathrm{X,Y}}$) regardless if atoms are covalently or QTAIM-bonded via an AIL. Furthermore, one can also determine the nature of the interaction, *e.g.* when $E_{\mathrm{int}}^{\mathrm{X,Y}} < 0$ then interaction is attractive. Additional insight on the physical character of an interaction can also be gained because $E_{\mathrm{int}}^{\mathrm{X,Y}}$ can be decomposed further into a classical (electrostatic) contribution, $V_{\mathrm{cl}}^{\mathrm{X,Y}}$, and exchange-correlation, XC, energy term, $V_{\mathrm{XC}}^{\mathrm{X,Y}}$ (which loosely might be interpreted as a classical covalent contribution). These energy components are of great importance as one can use them to quantify and characterize, in principle, all interactions of interest in any molecular system, hence also in the complexes investigated here.

In the following sections, in search of additional insight on parameters controlling relative stability of molecules, we will investigate the interactions between atoms (i) which are traditionally viewed as chemically bonded, (ii) where there is likely to be lone pair repulsion, and (iii) where there has been contention with regards to the nature of certain interactions, all of which are present in the BeNTPA complex.

Interactions within the Coordination Sphere of the Complexes. Table S8 shows the interaction energies between all atoms (Be, N and O) in the coordination spheres in BeNTA and BeNTPA – selected MP2 interaction energies are shown in brackets. Although the data using the X3LYP does not recover exact values at the RMP2 level of theory, the trends are identical giving confidence to the X3LYP data.

All the Be–O and Be–N coordination bonds are dominated by a classical contribution, $V_{\mathrm{cl}}^{\mathrm{X,Y}}$, which is an order of magnitude larger than the exchange-correlation term, $V_{\mathrm{XC}}^{\mathrm{X,Y}}$. This contradicts the general notion of the mechanism of the coordination bonds formation which classically is interpreted as sharing of a donated electron pair between a donor atom (here N and O) and the central metal ion, as also found for other molecular systems.[8]

Table S8. IQA partitioning of two-bodied interaction energies in BeNTA and BeNTPA for selected interactions of interest using the RXL3YP wavefunction on the MP2 structures. Selected MP2 data are shown in brackets.

BeNTA				BeNTPA			
Interaction	$V_{cl}^{X,Y}$	$V_{XC}^{X,Y}$	$E_{int}^{X,Y}$	Interaction	$V_{cl}^{X,Y}$	$V_{XC}^{X,Y}$	$E_{int}^{X,Y}$
Be–N	–417.8 (–443.0)	–19.4 (–19.7)	–437.2 (462.6)	Be–N	–403.8 (–423.8)	–20.5 (–20.5)	–424.3 (–444.3)
Be–O13	–457.6 (–472.2)	–26.7 (–26.6)	–484.4 (–498.8)	Be–O22	–459.0 (–473.9)	–25.9 (–25.8)	–484.9 (–499.6)
Be–O15	–457.6	–26.7	–484.3	Be–O25	–458.9	–26.0	–484.9
Be–O19	–457.6	–26.8	–484.3	Be–O28	–459.0	–25.9	–484.9
Sum:	–1790.6	–99.6	–1890.2	Sum:	–1780.7	–98.3	–1879.0
N•••O13	210.4 (226.1)	–13.4 (–14.5)	196.9 (211.6)	N•••O22	193.7 (205.5)	–10.5 (–11.5)	183.2 (194.1)
N•••O15	210.3	–13.4	196.9	N•••O25	193.7	–10.5	183.2
N•••O19	210.5	–13.5	197.0	N•••O28	193.7	–10.5	183.2
O13•••O15	207.0 (–215.8)	–9.7 (–10.3)	197.3 (205.5)	O22•••O25	215.9 (225.1)	–11.7 (–12.5)	204.1 (212.7)
O15•••O19	207.0	–9.6	197.3	O25•••O28	216.0	–11.7	204.3
O13•••O19	206.9	–9.6	197.3	O22•••O28	216.0	–11.7	204.3
Sum:	1252.0	–69.3	1182.7	Sum:	1228.9	–66.8	1162.2
Total:	–538.5	–168.8	–707.5	Total:	–551.7	–164.9	–716.9

Focusing on the coordination bonds, we note that $E_{int}^{X,Y}$ is larger (more negative by about 40-50 kcal/mol) for the Be–O than the Be–N bonds in both complexes, indicating that the Be–O are significantly stronger. This correlates well with the general trends, for interatomic distances d(Be,O) < d(Be,N) and density at BCPs ρ_{BCP}(Be–O) > ρ_{BCP}(Be–N), found for these complexes. Interestingly, even though the strength of the Be–O coordination bonds might be considered as comparable between the two complexes, the somewhat weaker Be–O in BeNTA (by about 0.5 kcal/mol) are characterised by slightly higher density at the BCPs, by about 0.002 au. This also correlates with the reverse trend in the ρ_{BCP} *vs.* d(Be,O) relationship and reveals that the larger density accumulation in the interatomic bonding region is not synonymous with stronger interaction in a complex, multi-atomic and congested molecular environment. This implies that, although ρ_{BCP} appears to be mainly controlled by the properties of interacting atoms, the surrounding atoms might add/remove some density;

hence, a diatomic interaction might not necessarily imply an entirely localized event. On the other hand, the slightly more covalent character of the Be–O in BeNTA, as measured by the $|V(r)|/G(r)$ ratio, is fully recovered by smaller classical term $V_{\mathrm{cl}}^{\mathrm{X,Y}}$ and, on average, slightly larger $V_{\mathrm{XC}}^{\mathrm{X,Y}}$ contribution. Furthermore, the Be–N bond of BeNTA is stronger than that in BeNTPA because $E_{\mathrm{int}}^{\mathrm{Be,N}}$ is significantly more negative by –14 kcal/mol. Hence, if one were to limit themselves to the properties of the coordination bonds, BeNTA would be predicted as the preferentially formed complex, a contradiction to what is known experimentally.

The repulsive interactions within the coordination spheres (N--O and O--O) of the BeNTA and BeNTPA complexes are dominated almost entirely by the electrostatic component (the XC-term contributes only ~5%). These interactions show two opposite trends; on average, $E_{\mathrm{int}}^{\mathrm{N,O}}$ is larger in BeNTA by ~16.7 kcal/mol whereas $E_{\mathrm{int}}^{\mathrm{O,O}}$ is larger in BeNTPA by ~9 kcal/mol. This correlates well with the observed interatomic distances, d(N,O) is shorter in BeNTA by ~0.2 Å and d(O,O) is longer by ~0.1 Å. Clearly, a mixed picture emerges from the analyses of $E_{\mathrm{int}}^{\mathrm{X,Y}}$ as well as interatomic distances. To gain deeper understanding, we summed up all the interaction energies between Be, N and O atoms. The sum of these interaction energies is –707.5 and –716.9 kcal/mol for BeNTA and BeNTPA respectively suggesting that there is a net stabilization in the coordination sphere in favour of BeNTPA. This can be seen as the first quantitative and conclusive finding in support of preferential formation of BeNTPA relative to BeNTA.

Furthermore, it is now possible to quantify specific energy contributions and we found that (i) four coordination bonds have a more stabilizing contribution (–1890 and –1879 kcal/mol in BeNTA and BeNTPA, respectively) than six steric clashes in the coordination sphere, N--O and O--O, which contributed 1183 and 1162 kcal/mol in BeNTA and BeNTPA, respectively, which explains why these complexes are formed, (ii) the total energy contribution made by coordination bonds in BeNTA is larger (more stabilizing) by ~–11 kcal/mol, and (iii) the total destabilizing contribution made by steric contacts (N--O and O--O) is smaller in BeNTPA by ~20 kcal/mol. Importantly, the difference of the $\Sigma E_{\mathrm{int}}^{\mathrm{X,Y}}$ values seen in Table 3.4 (BeNTPA – BeNTA) of –9.4 kcal/mol correlates well with the electronic energy for the competition reaction (–3.4 kcal/mol at X3LYP, which is comparable with experimentally observed $\Delta\log K_1$) and, at the same time, points at coordination sphere as the main contributor to the relative stability of these complexes. However, this contribution must be partly compensated by some other unfavourable sources of energy which most likely should be located outside the coordination sphere.

Interactions Outside the Coordination Sphere of the Complexes. Recalling that the NCI isosurfaces revealed the presence of additional interactions, CH•••HC and CH•••O, but only in the BeNTPA complex, it was of importance to explore their natures and quantify their contributions to the overall energy of this complex – relevant data are shown in Table 3.5. Looking at CH•••O, we found that the interaction energy $E_{\text{int}}^{\text{H,O}}$ is –5.0 kcal/mol; hence these three attractive interactions contribute about –15 kcal/mol in a stabilizing manner. Furthermore, as one would expect, this interaction is dominated by the classical term, $V_{\text{cl}}^{\text{H,O}}$ = –3.7 kcal/mol - see Table S9. Considering the CH•••HC interactions, because $V_{\text{cl}}^{\text{H,O}}$ 0.1 kcal/mol and $V_{\text{XC}}^{\text{H,H}}$ term of –2.3 kcal/mol dominates, they also appear to be of an overall stabilizing nature.

Table S9. IQA partitioning of two-bodied interaction energies in BeNTPA for intramolecular interactions identified by NCI isosurfaces using the XL3YP wavefunction on the MP2 structures.

Interaction	kcal/mol		
	$V_{\text{cl}}^{\text{X,Y}}$	$V_{\text{XC}}^{\text{X,Y}}$	$E_{\text{int}}^{\text{X,Y}}$
H6 ••• H12	0.1	–2.3	–2.2
H2 ••• H14	0.1	–2.3	–2.2
H10 ••• H16	0.1	–2.3	–2.2
H14 ••• O22	–3.7	–1.4	–5.0
H16 ••• O25	–3.7	–1.4	–5.0
H12 ••• O28	–3.7	–1.4	–5.0
Total:	–10.8	–11.1	–21.6

In order to insure that we had a correct qualitative description of these weak intramolecular interactions, some of them were analysed at the MP2 level of theory. Interestingly, the results predicted both interactions to contribute to the complex stability even more in stabilizing manner. Although we obtained $V_{\text{cl}}^{\text{H,H}}$ marginally larger (by ~0.1 kcal/mol) for the CH2•••H14C interaction, a significant increase in the $V_{\text{XC}}^{\text{H,H}}$ term resulted in an increase of an overall stabilizing contribution made, in absolute term by 0.3 kcal/mol. In case of the CH14•••O22 interaction, $V_{\text{cl}}^{\text{H,O}}$ and $V_{\text{XC}}^{\text{H,O}}$ of –4.4 and –1.6 kcal/mol, respectively, were found at MP2. This analysis not only shows that the CH•••HC interaction is only slightly repulsive and does appear to add to molecular stability, but also and importantly validates the usage of the X3LYP functional on the MP2-optimized structure. For both CH•••HC and CH•••O interactions in the BeNTPA complex, it is important to note that: (i) there are no AILs present, (ii) both show a blue region of concentration, an NCI indicator of stabilizing interaction due to density accumulation, (iii) an adjacent red isosurface, indicative of density depletion within a pseudo ring formed due to density accumulation between interacting atoms, (iv) electron density which consistently decreases along the cross-section (Figure S5(b)), and finally (v) these interactions are characterized by the overall negative interaction energy. Thus, from the IQA perspectives, there is no evidence which suggests that firstly, the CH•••HC interaction is locally destabilizing (note that this would provide an additional reason for preferential BeNTA complex formation) and secondly, that the CH•••O and CH•••HC intramolecular interaction differ qualitatively in nature. The most significant difference between the two interactions arises in the relative contributions made by the classical term, where it is almost negligible (but repulsive) for the CH•••HC interaction and attractive for the CH•••O interaction; in this respect, the IQA analysis recovered the common notion of these interactions' nature.

When the values of the interaction energy of the CH--HC and CH--O contacts are compared to those of (i) classically repulsive contacts in the coordination sphere (N--O and O--O), and (ii) coordination bonds, it is clear that the impact they have on the molecules' (in)stability is orders of magnitude smaller. On the other hand, the two intramolecular interactions, CH•••O and CH•••HC, contribute significantly to the overall stability of a molecule. When their total interaction energy contributions of –21.6 kcal kcal/mol is combined with that found from coordination spheres, –9.4 kcal/mol, the formation constant of BeNTPA would be expected to be much larger, by about 28 log units, which clearly is not the case (the experimental difference is about 2.4 log units only). This is another strong indication that there must be other and destabilizing energy components which must totally compensate contributions coming from the intramolecular CH•••HC and CH•••O interactions.

REFERENCES

[1] A. E. Martell; R. D. Hancock, *Metal Complexes in Aqueous Solutions*, Plenum Press: New York, 1996.

[2] R. D. Hancock; A. S. de Sousa; G. B. Walton; J. H. Reibenspies *Inorg. Chem.* **2007**, *46*, 4749.

[3] V. J. Thom; C. C. Fox; J. C. A. Boeyens; R. D. Hancock *J. Am. Chem. Soc.* **1984**, *106*, 5947.

[4] T. W. Hambley *J. Chem. Soc., Dalton Trans.* **1986**, 565.

[5] K. K. Govender; I. Cukrowski, *Inorg. Chem*. **2010**, *49*, 6931.

[6] I. Cukrowski; K. K. Govender; M. Mitoraj; M. Srebro *J. Phys. Chem. A* **2011**, *115*, 12746.

[7] R. F. W. Bader; H. Essen *J. Chem. Phys.* **1984**, *80*, 1943.

[8] I. Cukrowski; J. H. de Lange; M. Mitoraj *J. Phys. Chem. A* **2014**, *118*, 623.

[9] E. Espinosa; I. Alkorta; J. Elguero; E. Molins, *J. Chem. Phys.* **2002**, *117*, 5529.

[10] R. Flaig; Koritsanszky, B. Dittrich,; A.Wagner; P. Luger *J. Am. Chem. Soc.* **2002**, *124*, 3407.

[11] P. R. Varadwaj; I. Cukrowski; C. B. Perry; H. M. Marques *J. Phys. Chem. A* **2011**, *115*, 6629.

[12] A. M.Pendás; E. Francisco; M. A. Blanco; C. Gatti *Chem.–Eur. J*. **2007**, *13*, 9362.

[13] E. R. Johnson; S. Keinan; P. Mori-Sánchez; J. Contreras-García; A. J. Cohen; W. Yang, *J. Am. Chem. Soc.* **2010**, *132*, 6498.

[14] J. Contreras-García; E. R. Johnson; S. Keinan; R. Chaudret; J. P. Piquemal; D. Beratan; W. Yang *J. Chem. Theory Comput.* **2011**, *7*, 625.

[15] N. Gillet; R. Chaudret; J. Contreras-García; W. Yang; B. Silvi; J. P. Piquemal *J. Chem. Theory Comput.* **2012**, *8*, 3993.

[16] J. Contreras-García; W. Yang; E. R. Johnson *J. Phys. Chem. A* **2011**, *115*, 12983.

[17] J. R. Lane; J. Contreras-Garcia; J. Piquemal; B.J. Miller; Kjaergaard. *J. Chem. Theory Comput.* **2013**, *9*, 3263.

[18] Varadwaj, P. R.; Varadwaj, A.; Peslherbe, G. H.; Marques H. M. *J. Phys. Chem. A.* **2011**, *115*, 13180–13190.

[19] M. A. Blanco; A. M. Pendás; E. Francisco *J. Chem. Theory Comput.* **2005**, *1*, 1096.

[20] E. Francisco; A. M. Pendás; M. A. Blanco *J. Chem. Theory Comput.* **2006**, *2*, 90.

[21] A. M. Pendás; M. A. Blanco; E. Francisco *J. Comput. Chem.* **2006**, *28*, 161.

Table S10. Cartesian coordinates of the NTA ligand at the RMP2 level of theory. Cartesian coordinates are identical for all SPFCs thus only molecular energies are provided).

Centre Number	Atomic Number	Atomic Type	Coordinates (Å)		
			X	Y	Z
1	6	0	0.8152	–1.1007	–0.5133
2	1	0	0.3029	–2.0394	–0.2714
3	1	0	0.9079	–1.0582	–1.6166
4	7	0	–0.0005	0.0000	–0.0165
5	6	0	–1.3636	–0.1543	–0.5080
6	1	0	–1.9190	0.7580	–0.2595
7	1	0	–1.3787	–0.2495	–1.6119
8	6	0	0.5462	1.2573	–0.5102
9	1	0	0.4644	1.3176	–1.6133
10	1	0	1.6153	1.2807	–0.2672
11	6	0	2.2406	–1.2170	0.0749
12	8	0	3.0428	–1.8938	–0.6357
13	8	0	2.4832	–0.6925	1.1940
14	6	0	–0.0637	2.5495	0.0805
15	8	0	–0.6303	2.4960	1.2039
16	8	0	0.1131	3.5827	–0.6324
17	6	0	–2.1763	–1.3325	0.0780
18	8	0	–3.1800	–1.6694	–0.6191
19	8	0	–1.8262	–1.8259	1.1823

Molecular Energy (MP2): –737.16095522 au

Molecular Energy (PBE1PBE): –738.22749526 au

Molecular Energy (B3LYP): –739.04403952 au

Molecular Energy (X3LYP): –738.75902221 au

Table S11. Cartesian coordinates of the NTPA ligand at the RMP2 level of theory. Cartesian coordinates are identical for all SPFCs thus only molecular energies are provided).

Centre Number	Atomic Number	Atomic Type	Coordinates (Å)		
			X	Y	Z
1	6	0	1.2809	0.5511	0.2217
2	1	0	1.2237	1.6420	0.1856
3	1	0	1.4409	0.2711	1.2818
4	7	0	0.0052	0.0006	–0.2574
5	6	0	–1.1100	0.8298	0.2208
6	1	0	–2.0257	0.2333	0.1828
7	1	0	–0.9487	1.1069	1.2813
8	6	0	–0.1577	–1.3796	0.2210
9	1	0	–0.4902	–1.3774	1.2778
10	1	0	0.8173	–1.8736	0.1947
11	6	0	–1.1332	–2.1932	–0.6318
12	1	0	–0.7008	–2.3058	–1.6319
13	6	0	–1.3215	2.0883	–0.6226
14	1	0	–1.6047	1.7770	–1.6338
15	6	0	2.4758	0.1052	–0.6226
16	1	0	2.3532	0.5164	–1.6308
17	1	0	2.5131	–0.9852	–0.6895
18	1	0	–0.3985	2.6714	–0.6770
19	1	0	–2.0906	–1.6723	–0.7169
20	6	0	3.7806	0.6332	–0.0036
21	8	0	3.9585	1.8852	–0.0642
22	8	0	4.5497	–0.2116	0.5409
23	6	0	–1.3475	–3.5762	0.0046
24	8	0	–2.4443	–3.7741	0.6049
25	8	0	–0.3840	–4.3916	–0.0937
26	6	0	–2.4410	2.9425	–0.0059
27	8	0	–2.0947	3.9834	0.6256
28	8	0	–3.6207	2.5068	–0.1526

Molecular Energy (MP2): –854.75183093 au

Molecular Energy (PBE1PBE): –856.05220453 au

Molecular Energy (B3LYP): –857.01889370 au

Molecular Energy (X3LYP): –856.66836563 au

Table S12. Cartesian coordinates of the BeNTA ligand at the RMP2 level of theory. Cartesian coordinates are identical for all SPFCs thus only molecular energies are provided).

Centre Number	Atomic Number	Atomic Type	Coordinates (Å)		
			X	Y	Z
1	6	0	0.1244	1.4342	1.1103
2	1	0	–0.8730	1.8534	1.2798
3	1	0	0.7274	1.6187	2.0039
4	7	0	–0.0022	–0.0007	0.7987
5	6	0	–1.3084	–0.6075	1.1109
6	1	0	–1.1732	–1.6803	1.2849
7	1	0	–1.7709	–0.1740	2.0022
8	6	0	1.1765	–0.8278	1.1123
9	1	0	1.0300	–1.4471	2.0019
10	1	0	2.0368	–0.1740	1.2908
11	6	0	0.7203	2.1518	–0.1170
12	8	0	1.1644	3.2924	–0.0128
13	8	0	0.6626	1.4487	–1.2136
14	6	0	1.5074	–1.6976	–0.1168
15	8	0	0.9256	–1.2988	–1.2135
16	8	0	2.2802	–2.6469	–0.0128
17	6	0	–2.2262	–0.4537	–0.1179
18	8	0	–3.4360	–0.6413	–0.0152
19	8	0	–1.5873	–0.1520	–1.2136
20	4	0	–0.0003	–0.0011	–0.9735

Molecular Energy (MP2): –751.80525159 au

Molecular Energy (PBE1PBE): –752.89579597 au

Molecular Energy (B3LYP): –753.73210727 au

Molecular Energy (X3LYP): –753.44050911 au

Table S13. Cartesian coordinates of the BeNTPA ligand at the RMP2 level of theory. Cartesian coordinates are identical for all SPFCs thus only molecular energies are provided).

Centre Number	Atomic Number	Atomic Type	Coordinates (Å)		
			X	Y	Z
1	6	0	1.3893	–0.1999	1.6210
2	1	0	1.8901	0.7725	1.6261
3	1	0	1.3388	–0.5534	2.6594
4	7	0	0.0003	–0.0002	1.1157
5	6	0	–0.5217	1.3021	1.6216
6	1	0	–1.6143	1.2487	1.6271
7	1	0	–0.1900	1.4348	2.6598
8	6	0	–0.8663	–1.1037	1.6214
9	1	0	–1.1470	–0.8832	2.6599
10	1	0	–0.2735	–2.0228	1.6264
11	6	0	–2.1008	–1.3054	0.7448
12	1	0	–2.6199	–0.3525	0.5841
13	6	0	–0.0791	2.4720	0.7446
14	1	0	1.0055	2.4441	0.5828
15	6	0	2.1800	–1.1685	0.7435
16	1	0	1.6123	–2.0930	0.5812
17	1	0	3.1137	–1.4385	1.2423
18	1	0	–0.3135	3.4150	1.2438
19	1	0	–2.7996	–1.9809	1.2438
20	6	0	2.4990	–0.5523	–0.6158
21	8	0	3.6194	–0.6801	–1.1179
22	8	0	1.5275	0.1145	–1.1717
23	6	0	–1.7282	–1.8875	–0.6157
24	8	0	–2.4007	–2.7922	–1.1187
25	8	0	–0.6648	–1.3800	–1.1715
26	6	0	–0.7711	2.4405	–0.6152
27	8	0	–1.2205	3.4750	–1.1168
28	8	0	–0.8623	1.2660	–1.1717
29	4	0	0.0001	0.0001	–0.6751

Molecular Energy (MP2): –869.41010958 au

Molecular Energy (PBE1PBE): –870.72792430 au

Molecular Energy (B3LYP): –871.71119060 au

Molecular Energy (X3LYP): –871.35521466 au

Table S14. Computed preorganization (strain) energies and binding energies using $\mathcal{L}_f$ of NTA and NTPA, the complexes BeNTA and BeNTPA, and the respective $L_{p\text{-}org}$.

Level of Theory	$G_{p\text{-}org}$				G_{aff}				ΔG_{ML} [a]
	NTA	NTPA	$\Delta G_{p\text{-}org}$ [b]	Ratio[c]	BeNTA	BeNTPA	ΔG_{bind} [d]	Ratio[c]	
MP2[e]	53.8	65.0	11.2	1.2	–252.6	–270.3	–17.6	1.1	–6.4

[a] $\Delta G_{ML} = G_{BeNTPA} – G_{BeNTA}$; [b] $\Delta G_{p\text{-}org} = G_{p\text{-}org}(NTPA) – G_{p\text{-}org}(NTA)$; [c] Ratio = (NTPA/NTA) value; [d] $\Delta G_{bind} = G_{bind}(BeNTPA) – G_{bind}(BeNTA)$; [e] energies were obtained by optimizing the lowest energy conformer of each molecule.

Table S15. Computed affinity energies using the complexes BeNTA and BeNTPA, and the respective $L_{p\text{-}org}$.

Level of Theory	E [a]					E_{aff} [b]	
	Be	$NTA_{p\text{-}org}$	BeNTA	$NTPA_{p\text{-}org}$	BeNTPA	BeNTA	BeNTPA
MP2	–14.3024	–737.0781	–751.8053	–854.6543	–869.4101	–266.5	–284.5
PBE1PBE*	–14.3326	–738.1418	–752.8958	–855.9443	–870.7279	–264.4	–283.0
B3LYP*	–14.3450	–738.9588	–753.7321	–856.9082	–871.7112	–268.8	–287.4
X3LYP*	–14.3353	–738.6742	–753.4405	–856.5590	–871.3552	–270.5	–289.2

[a] values are in au; [b] values are in kcal/mol

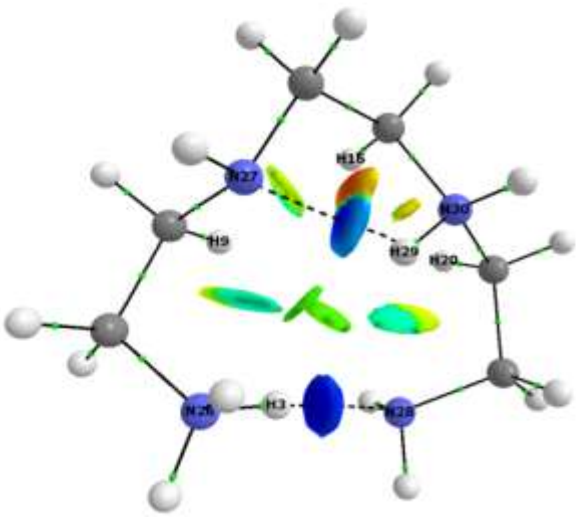

Figure S6. Typical NCI blue-coloured isosurface between H3 and N28 which recovers a classical intramolecular NH•••N hydrogen bond.